JACK N. AVERITT COLLEGE of GRADUATE STUDIES GEORGIA SOUTHERN UNIVERSITY

Georgia Southern University

Digital Commons@Georgia Southern

Electronic Theses and Dissertations

Graduate Studies, Jack N. Averitt College of

Spring 2017

Electroencephalographic Signal Processing and Classification Techniques for Noninvasive Motor Imagery Based Brain Computer Interface

Md Erfanul Alam

Follow this and additional works at: https://digitalcommons.georgiasouthern.edu/etd

Part of the Acoustics, Dynamics, and Controls Commons, and the Biomechanical Engineering Commons

Recommended Citation

Alam, Md Erfanul, "Electroencephalographic Signal Processing and Classification Techniques for Noninvasive Motor Imagery Based Brain Computer Interface" (2017). *Electronic Theses and Dissertations*. 1591.
https://digitalcommons.georgiasouthern.edu/etd/1591

This thesis (open access) is brought to you for free and open access by the Graduate Studies, Jack N. Averitt College of at Digital Commons@Georgia Southern. It has been accepted for inclusion in Electronic Theses and Dissertations by an authorized administrator of Digital Commons@Georgia Southern. For more information, please contact digitalcommons@georgiasouthern.edu.

ELECTROENCEPHALOGRAPHIC SIGNAL PROCESSING AND CLASSIFICATION TECHNIQUES FOR NONINVASIVE MOTOR IMAGERY BASED BRAIN COMPUTER INTERFACE

by

MD ERFANUL ALAM

(Under the Direction of Biswanath Samanta)

ABSTRACT

In motor imagery (MI) based brain-computer interface (BCI), success depends on reliable processing of the noisy, non-linear, and non-stationary brain activity signals for extraction of features and effective classification of MI activity as well as translation to the corresponding intended actions. In this study, signal processing and classification techniques are presented for electroencephalogram (EEG) signals for motor imagery based brain-computer interface. EEG signals have been acquired placing the electrodes following the international 10-20 system. The acquired signals have been pre-processed removing artifacts using empirical mode decomposition (EMD) and two extended versions of EMD, ensemble empirical mode decomposition (EEMD), and multivariate empirical mode decomposition (MEMD) leading to better signal to noise ratio (SNR) and reduced mean square error (MSE) compared to independent component analysis (ICA). EEG signals have been decomposed into independent mode function (IMFs) that are further processed to extract features like sample entropy (SampEn) and band power (BP). The extracted features have been used in support vector machines to characterize and identify MI activities. EMD and its variants, EEMD, MEMD have been compared with common spatial pattern (CSP) for different MI activities. SNR values from EMD, EEMD and MEMD (4.3, 7.64, 10.62) are much better than ICA (2.1) but accuracy of MI activity identification is slightly better for

ICA than EMD using BP and SampEn. Further work is outlined to include more features with larger database for better classification accuracy.

Index Words: Brain computer interface, Common spatial pattern, Empirical mode decomposition, Independent component analysis, Support vector machine

ELECTROENCEPHALOGRAPHIC SIGNAL PROCESSING AND CLASSIFICATION TECHNIQUES FOR NONINVASIVE MOTOR IMAGERY BASED BRAIN COMPUTER INTERFACE

by

MD ERFANUL ALAM

B.S., Bangladesh University of Engineering and Technology, Bangladesh, 2014

M.S., Georgia Southern University, 2017

A Thesis Submitted to the Graduate Faculty of Georgia Southern University in Partial Fulfillment

of the Requirements for the Degree

MASTER OF SCIENCE

STATESBORO, GEORGIA

©2017

MD ERFANUL ALAM

All Rights Reserved

ELECTROENCEPHALOGRAPHIC SIGNAL PROCESSING AND CLASSIFICATION TECHNIQUES FOR NONINVASIVE MOTOR IMAGERY BASED BRAIN COMPUTER INTERFACE

by

MD ERFANUL ALAM

Major Professor: Biswanath Samanta

Committee: Minchul Shin

JungHun Choi

Electronic Version Approved:

May 2017

DEDICATION

This thesis is dedicated to my beloved family.

ACKNOWLEDGMENTS

First of all I express my profound gratitude to my thesis supervisor, Dr. Biswanath Samanta, Department of Mechanical Engineering, Georgia Southern University for enlightening me about the utmost importance of Brain Computer Interface research. Without his continuous supervision, guidance, thoughtful suggestions and valuable advice, this work would not have been possible. I am grateful to all of those who have voluntarily helped me in research by being a subject for data acquisition during this research. I also thank my parents and all family members for their encouragement and love during my course of work. Lastly, I express my gratitude to Georgia Southern University library. Many reference papers and books which were necessary for this thesis work had been issued from the library.

TABLE OF CONTENTS

Page

DEDICATION 2

ACKNOWLEDGMENTS 3

LIST OF FIGURES 8

CHAPTER

1 INTRODUCTION 11

1.1 Motor Imagery Based Brain-Computer Interface 11

1.2 Objectives and Scope of the Present Work 12

1.3 Organization of the Thesis 13

2 LITERATURE REVIEW 15

2.1 Measurement of Brain Activity Signals 15

2.2 Invasive and Non- Invasive BCI 16

2.3 Electroencephalography (EEG) 17

2.4 Motor Imagery Based BCI 20

2.5 Components of an EEG System 22

2.5.1 Preprocessing 22

2.5.1.1 EEG Artifacts 22

2.5.2 Feature Extraction 25

2.5.2.1 Optimal Feature Extraction 26

2.5.2.2 Common Spatial Pattern 27

2.5.2.3 Empirical Mode Decomposition (EMD) and Its Variants 28

2.5.3 Classification 29

3 METHODOLOGY 32

3.1 EEG System 32

3.1.1 Hardware 34

3.1.1.1 Electrodes 34

3.1.1.2 Skin preparation kits 34

3.1.1.3 Amplifier 35

3.1.2 Software 36

3.1.2.1 BCI2000 36

3.2 Data Acquisition 38

3.3 Signal Processing Algorithms 39

3.3.1 Independent Component Analysis 39

3.3.2 Empirical Mode Decomposition (EMD) 40

3.3.3 Ensemble Empirical Mode Decomposition 43

3.3.4 Multivariate Empirical Mode Decomposition 43

3.3.5 Performance Evaluation 44

3.4 Feature Selection Algorithm 45

3.4.1 R square Coefficient Method 45

3.4.2 Common Spatial Pattern 46

3.4.3 Sample Entropy 48

3.4.4 Band Power 50
3.5 Classification 50
3.5.1 Support Vector Machine 50
4 RESULTS AND DISCUSSION 53
4.1 Acquired EEG Signals 53
4.2 Artifact Removal 53
4.2.1 Power Line Noise Removal 54
4.2.2 Eye Blink Artifact Removal 58
4.3 Feature Extraction 66
4.3.1 Spectral Power 66
4.3.1.1 Right Hand Movement 67
4.3.1.2 Left Hand Movement 67
4.3.1.3 Both Hands Movement 71
4.3.1.4 Both Feet Movement 71
4.3.1.5 Comparison Between Actual Movement and Imagined Movement 74
4.3.2 EMD Based Feature Selection 75
4.3.2.1 Band Power 75
4.3.2.2 Sample Entropy 77
5 CONCLUSION 83
5.1 Summary of Present Work 83
5.2 Scope For Future Work 84

REFERENCES 86

LIST OF FIGURES

Figure Page

2.1 Signal acquisition methods for Brain Computer Interface 17

2.2 different brain rhythms as measured by EEG [1] 19

2.3 Basic design and operation of any BCI system 22

2.4 Artifacts associated with EEG signal [2] 24

2.5 Different types of Classifiers used in BCI 30

2.6 SVM finds the optimal hyperplane for generalization [3]. 30

3.1 International 10-20 system for electrode placement [4] 33

3.2 Data Acquisition accessories (a) Electrode (b) Conductive gel (c) Skin preparation gel and (d) SynAmps RT Amplifier 35

3.3 Four modules of BCI2000 37

3.4 Photographs during the process of acquisition of EEG signal acquisition 38

3.5 Flow chart of Empirical Mode Decomposition algorithm 42

3.6 Optimal feature extraction based on R-square coefficient method . . . 47

3.7 Linearly separable SVM technique 52

4.1 Acquired EEG signals with different artifacts 54

4.2 Power spectrum of acquired signals (a) channels F4, C3, C4 and P3 (b) channels P4, F7, F8 and T3 55

4.3 EEG signals and IMFs (a) C3 signal (right hand movement) (First graph in the figure is the original signal and the last one is residue, remaining are IMFs 1 to 12(top to bottom) (b) C4 signal (left hand movement. (First graph in the figure is the original signal and the last one is residue, remaining are the IMFs 1 to 12(top to bottom)) 56

4.4 Power spectra of IMFs (a) channel C3 (b) channel C4 57

4.5 Reconstructed EEG signals after power line artifact removal 58

4.6 Contaminated EEG from Fp1 channel 59

4.7 Empirical Mode Decomposition of Fp1 channel 59

4.8 Sample entropy of channels Fp1 and Fp2 60

4.9 Corrected signal of Fp1 channel 61

4.10 Reconstructed EEG signals after removal of artifacts 61

4.11 Signal to noise ratio (SNR) of EEG signals for channels C3, Cp1, Cp3, C4, Cp2, Cp4 for three subjects (a) Subject 1 (b) Subject 2 (c) Subject 3 . . 62

4.12 Mean Square Error (MSE) of EEG signals for channels C3, Cp1, Cp3, C4, Cp2, Cp4 for three subjects (a) Subject 1 (b) Subject 2 (c) Subject 3 . . 63

4.13 IMFs of EEG signal for channel C3 (a) EEMD, and (b) MEMD . . . 64

4.14 Spectral power of IMFs obtained by (a) EMD (b) EEMD and (c) MEMD 65

4.15 Signal to noise ratio (SNR) of EEG signals from channels C3, Cp1, Cp3, C4 Cp2, Cp4 for three algorithms : EMD, EEMD, MEMD 66

4.16 Spectral power density of EEG signals from channels (a)C1 (b)Cp1 (c)Cp3 and (d)C3 67

4.17 Spectral power density of EEG signals from channels (a)C2 (b)Cp2 (c)Cp4 and (d)C4 68

4.18 R square of Right hand movement at different frequencies 69

4.19 R square of Left hand movement at different frequencies 70

4.20 R square topography corresponds to (a)right hand movement at 16 Hz (b)left hand movement at 14 Hz 70

4.21 Spectral power density EEG signals for both hands movement (a)channel C3 and (b)channel C4 71

4.22 R square of Both hands movement at 14 Hz 72

4.23 Spectral power density of channel for both feet movement(a)C1 (b) Cz and (b)Cpz 73

4.24 R square of Both feet movement at 10 Hz 73

4.25 Spectral power density for imagined(a)right hand movement (b) left hand movement 74

4.26 Spectral power density for imagined both hands movement 75

4.27 Intrinsic mode functions of (a) channel C3 (b) channel C4 76

4.28 PSD (dB/Hz) vs. frequency (Hz) of each IMF for channel C3 (a) actual movement and (b) imagined movement 78

4.29 PSD (dB/Hz) vs. frequency (Hz) of each IMF for channel C4 (a) actual movement and (b) imagined movement 79

4.30 Average accuracy using Band power (BP) as feature for four tasks . . 80

4.31 Average accuracy using Sample Entropy (SampEn) as feature for four tasks 81

4.32 Comparison of CSP and EMD feature extraction technique 82

CHAPTER 1

INTRODUCTION

1.1 Motor Imagery Based Brain-Computer Interface

As modern assistive technology has become more sophisticated transitioning from simple rigid objects intended to only help support the user's weight to mechatronic devices capable of complex reactive support and even motion, there is a growing need for enhanced user control. Now that the hardware is sufficiently advanced, research has shifted focus to technology that allows human to communicate more easily with the devices to modify or control the behavior. One of the foremost methods for interacting with these assistive devices is Brain-Computer Interfacing (BCI). Brain-computer interfaces (BCIs) are a special type of exocortex used to interact with the environment via neural signals [5]. An exocortex is a wearable (or implanted) computer used to augment a brain's biological high-level cognitive processes and inform a user's decisions and actions. The messages and commands sent through a BCI are encoded into the user's brain activity. Brain computer interfaces (BCIs) can be broadly classified in two types, invasive: where electrodes are embedded into the brain surgically and non-invasive: where the measurement sensors are placed outside the head, on the scalp, for instance. Most noninvasive BCIs are based on electroencephalography (EEG) that measures and records the scalp electrical activity generated by brain.

Imagining a movement or performing an action mentally without moving a limb is known as Motor Imagery (MI). The Motor imagery produces similar effects on the brain rhythm in the sensory-motor cortex as the real executed movement [6]. Motor imagery based BCI (MI-BCI), that is, the imagination of a motor action without any actual movement of limbs, has clear practical significance, especially in neurological and mobility rehabilitation [7]. Mobility rehabilitation is a form of physical rehabilitation used with patients who have mobility issues, to restore their lost functions and regain previous levels of mobility or

at least help them adapt to their acquired disabilities. In MI based BCI, a movement could be detected from the EEG signals recorded from the appropriate position on the cortex [8]. Measured electroencephalography (EEG) signals can be contaminated with artifacts from other electrophysiological signal sources which are non-cerebral in origin. This contamination decreases accuracy of neuroengineering applications such as MI-BCI. Moreover, EEG signals are weak, nonlinear and non-stationary. Suitable signal processing algorithms are essential to process EEG signals for artifact removal, feature extraction, identification and classification of MI activities in successful applications of MI-BCI.

1.2 Objectives and Scope of the Present Work

The main hypothesis of this study is: if suitable algorithms are used for artifact removal and feature extraction from motor imagery based EEG signals, the signal to noise ratio (SNR) of pre-processed EEG signals will improve leading to distinct features for better identification and classification of MI-BCI activities. To test the hypothesis, a fully data-driven time-frequency analysis technique namely, empirical mode decomposition (EMD) [9] has been used to process the noisy, weak, nonlinear and non-stationary motor imagery EEG signals. Two extended versions of EMD, namely ensemble empirical mode decomposition (EEMD) [10] and multivariate empirical mode decomposition (MEMD) [11] have been used and compared with common spatial pattern (CSP) of BCI2000 [12]. To test the hypothesis, the following objectives were set in this work:

- Removal of artifacts from the raw EEG signals acquired for different actual motor actions and MI activities.
- Comparison of performance of EMD and its variants, EEMD and MEMD with the CSP based approach for artifact removal.
- Extraction of features (r square coefficient, spectral power, band power and sample

entropy)from the pre-processed EEG signals for motor task identification.

- Identification and classification of actual motor actions and MI activities using extracted features.

- Comparison of accuracy of mental task identification for EMD and CSP based approaches.

To achieve these objectives, experiments were set up with the EEG system in Bio-Inspired Robotics and Intelligent Systems (B-IRIS) lab. Three voluntary subjects were used to acquire EEG signals. A programmed instruction was given to them to maintain a sequence for doing their motor tasks. EEG signals were preprocessed for artifact removal. Two levels of artifact removal were associated with the EEG signals, namely, power line noise removal and eye blink artifact removal. Two features, namely band power (BP) and sample entropy (SampEn) were extracted from the reconstructed EEG signals after removal of artifacts. Extracted features were used for identification and classification of different MI activities.

1.3 Organization of the Thesis

The rest of thesis is organized as follows. In Chapter 2 a review of literature relevant to the area of this research is presented. First the fundamentals of BCI and measurement of brain activity EEG signals of a subject to operate a BCI system are discussed. The oscillatory nature of brain signals and corresponding frequency bands are described next. It is followed with a discussion on the origins of artifacts found in EEG signals and the process of artifact removal. Finally, different feature extraction techniques are presented along with a brief discussion on classification techniques.

In Chapter 3 the methodology used in this study is presented. First a description of EEG system along with the type of electrodes, the brain cap, Synamps RT amplifier and filter

are discussed. Next the data acquisition system using BCI2000 is presented. The signal processing algorithms which are used to remove the artifacts from the raw EEG signal are described next. Finally, feature extraction and classification algorithms that are used in this study are discussed.

In Chapter 4 the results of this study are presented. The acquired EEG signals for different motor activities are presented first. Next identification of artifacts in EEG signals and removal of artifacts are presented using the signal processing techniques of EMD and the extensions, EEMD and MEMD. It is followed with presentation of performance results of signal to noise ratio (SNR) and mean square error (MSE) for the signal processing algorithms based on EMD and CSP. Next results of extraction of features like r square coefficient, spectral power, band power and sample entropy are discussed. Finally, results of identification and classification accuracy of the actual and the imagined motor tasks with support vector machine (SVM) are presented.

In Chapter 5 the main features of the present work are summarized first. The chapter is concluded with an outline of scope of future extensions of the work.

CHAPTER 2

LITERATURE REVIEW

Brain computer interfaces (BCIs) are aimed at restoring crucial functions to people who are severely disabled by a wide variety of neuromuscular disorders, and at enhancing functions in healthy individuals. Significant advances have been made in the development of BCIs where intracranial electrophysiological signals are recorded and interpreted to decode the intent of subjects and control external devices [13, 14]. Noninvasive BCIs have also long been pursued from scalp recorded noninvasive electroencephalograms (EEGs). Among such noninvasive BCIs, sensorimotor rhythm (SMR)-based BCIs have been developed using a motor imagery paradigm [15, 16]. The efficacy of noninvasive SMR-based BCIs is supported by research indicating that the ability to generate SMRs remains present in users with other neurodegenerative disorders such as muscular dystrophy and spinal muscular atrophy [17].

2.1 Measurement of Brain Activity Signals

The first step required to operate a BCI involves measuring the subject's brain activity signals. Different kinds of brain signals, that are easily observable and controllable, have been identified as suitable for a BCI [5]. Various techniques for measuring brain activity signals within a BCI [18] include, Magnetoencephalography (MEG) [19, 20], functional Magnetic Resonance Imaging (fMRI) [21], Near InfraRed Spectroscopy (NIRS) [22], and Electrocorticography (ECoG) [23] or implanted electrodes, placed under the skull. Figure 2.1 shows some of these techniques. However, the widely used technique is ElectroEncephaloGraphy (EEG) [18] as EEG is non-invasive, relatively less expensive and provides a good time resolution. Consequently, most current BCI systems are based on EEG to measure brain activity signals. Thus, in this thesis work, EEG based BCI design has been considered.

Oscillatory activity-based BCI techniques make use of both spatial and spectral information through changes in power in some specific frequency bands, in some specific brain areas. As an example, a basic design for a motor-imagery BCI would exploit the spatial information by extracting features only from EEG channels localized over the motor areas of the brain, typically channels C3 for right hand movements, Cz for foot movements and C4 for left hand movements. It would exploit the spectral information by focusing on frequency bands μ (8 to 12 Hz) and β (16 to 24 Hz). More precisely, for a BCI that can recognize left hand MI versus right hand MI, the basic features extracted would be the average band power in 8 to 12 Hz and 16 to 24 Hz from both channels C3 and C4. Therefore, the EEG signals would be described by only 4 features. There are many ways to compute band power features from EEG signals [24]. However, a simple, popular and efficient one is to first band-pass filter the EEG signal from a given channel into the frequency band of interest, then to square the resulting signal to compute the signal power, and finally to average it over time.

2.2 Invasive and Non- Invasive BCI

Though EEG is the most widely used type of signals in BCI, it should be noted that a large and rapidly growing part of BCI research is dedicated to the use of implanted electrodes which measure the activity of groups of neurons [1, 25]. Figure 2.1 shows two basic kinds of brain computer interfaces and signals that could be recorded from these types. Implanted electrodes make it possible to obtain signals with a much better quality and a much better spatial resolution than with non-invasive methods [26]. Some invasive methods can measure the activity of single neurons while a non-invasive method such as EEG measures the resulting activity of thousands of neurons. As such, it is suggested that invasive BCI could obtain better results, in terms of performances than non-invasive methods, and especially than EEG. However, this statement still needs to be confirmed and

is still a topic of debate within the BCI community. Indeed, even if EEG-based BCI are based on much noisier and coarser signals than those of invasive BCI, some studies have reported that they can reach similar information transfer rates [27]. The main drawback of invasive BCI is precisely the fact that they are invasive, which requires that the subject endures a surgery operation in order to use the system. Moreover, implanted electrodes have a limited lifetime, which makes the subject endure regular surgery operations in order to replace the electrodes. Then, the use of implanted electrodes might be dangerous for the health of the subjects. Finally, implanting electrodes in a human brain also raises numerous ethics problems. These points make non-invasive BCI, and especially EEG-based BCI, the most widely used and the most popular.

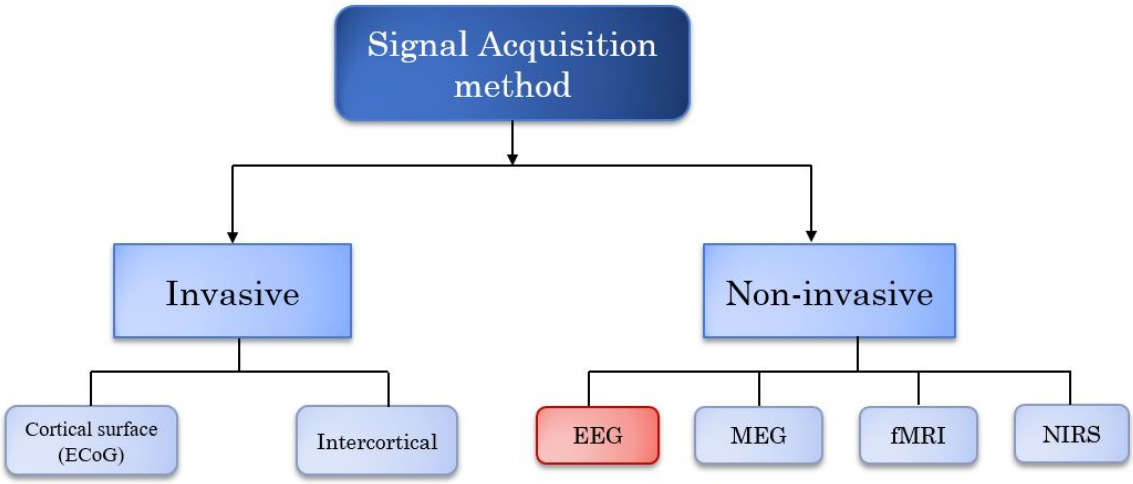

Figure 2.1: Signal acquisition methods for Brain Computer Interface

2.3 Electroencephalography (EEG)

Electroencephalography measures and records the electrical activity generated by the brain using electrodes placed on the scalp. EEG measures the sum of the post-synaptic potentials generated by thousands of neurons having the same radial orientation with respect to the

scalp. The first EEG measurements on a human subject have been conducted in 1924 by Hans Berger. It is at that time that he worked out the name of electroencephalogram. His fundamental discovery was published in 1929 [28]. Signals recorded by EEG have a very weak amplitude, in the order of some microvolts. It is thus necessary to strongly amplify these signals before digitizing and processing them. Typically, EEG signals measurements are performed using a number of electrodes which varies from 1 to about 256, these electrodes being generally attached using an elastic cap. The contact between the electrodes and the skin is generally enhanced by the use of a conductive gel or paste. This makes the electrode montage procedure a generally tedious and lengthy operation. It is interesting to note that BCI researchers have recently proposed and validated dry electrodes for BCI, that is, electrodes which do not require conductive gels or pastes for use [29]. However, the performance of the resulting BCI (in terms of maximum information rate) were, on average, 30% lower than the one obtained with a BCI based on electrodes that use conductive gels or pastes. Electrodes are generally placed and named according to a standard model, namely, the 10- 20 international system [30].

EEG signals are composed of different oscillations named rhythms [1]. These rhythms have distinct properties in terms of spatial and spectral localization. There are 6 classical brain rhythms shown in figure 2.2

- Delta (δ) rhythm: This is a slow rhythm (1-4 Hz), with a relatively large amplitude, which is mainly found in adults during a deep sleep.

- Theta (θ) rhythm: This a slightly faster rhythm (4-7 Hz), observed mainly during drowsiness and in young children.

- Alpha (α) rhythm: These are oscillations, located in the 8-12 Hz frequency band, which appear mainly in the posterior regions of the head (occipital lobe) when the subject has closed eyes or is in a relaxation state.

- Mu (μ) rhythm: These are oscillations in the 8-13 Hz frequency band, being located in the motor and sensorimotor cortex. The amplitude of this rhythm varies when the subject performs movements. Consequently, this rhythm is also known as the sensorimotor rhythm.

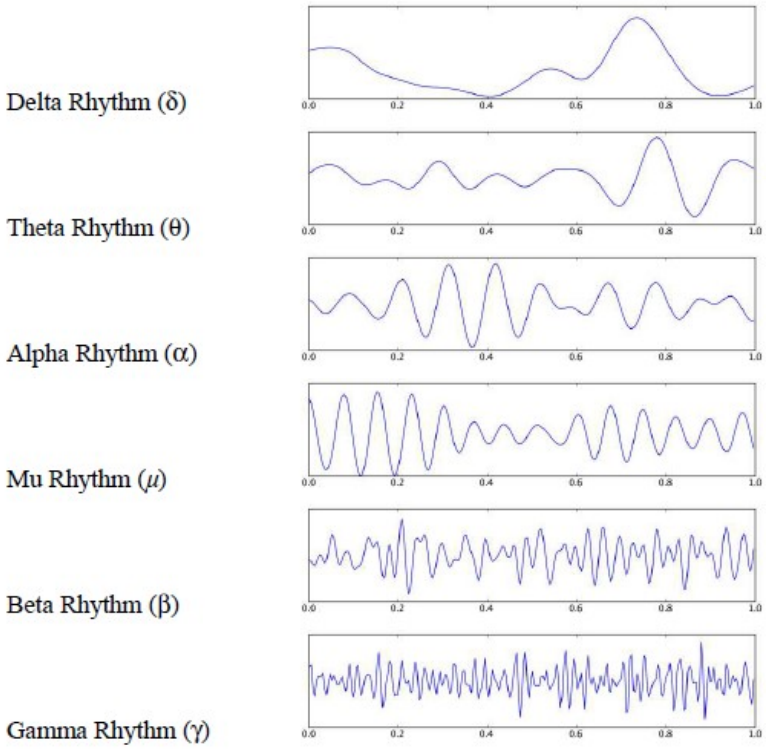

Figure 2.2: different brain rhythms as measured by EEG [1]

- Beta (β) rhythm: This is a relatively fast rhythm, belonging approximately to the 13-30 Hz frequency band. It is a rhythm which is observed in awaken and conscious persons. This rhythm is also affected by the performance of movements, in the motor areas.

- Gamma (γ) rhythm: This rhythm concerns mainly frequencies above 30 Hz. This rhythm is sometimes defined as having a maximal frequency around 80 Hz to 100 Hz. It is associated to various cognitive and motor functions.

2.4 Motor Imagery Based BCI

Whenever a muscle in the human body is voluntarily moved, oscillations occur in brain activity signals in the sensorimotor and motor areas, and the so called the sensorimotor rhythms (SMR) change. These changes are fairly localized, following the homuncular organization of this cortical region [31]. The decrease in oscillations is called event related desynchronization (ERD) and typically appears during movement or preparation of movement. The increase in oscillations is called event-related synchronization (ERS) and appears after movement or relaxation. In fact, even imagining such movements produces very similar ERD/ERS patterns as the actual movements would [32]. The neurophysiological basis for motor imagery BCI are μ (8 to 12 Hz) and β (16 to 24 Hz) rhythms in EEG [33], which have been observed in the central region of the brain when subjects plan and execute hand or finger movements [34, 35]. According to the homunculus representation of the body in the primary motor cortex, the motor cortex is divided into various parts controlling the movements of the body part represented by that section. Each side of the body is controlled by the contralateral hemisphere of the brain. Placing electrodes on the location of the representation of the required body part allows recording the brain activities related to the movement of that part. Motor imagery based BCI works by making the subject imagine the movement of certain limbs, like grasping with the left- or right hand or, moving the feet and measuring the ERD/ERS patterns over the respective cortical areas. Each imagined limb movement is associated with a certain action that gets executed when imagining the respective limb movement. Although the motor imagery paradigm seems very natural compared to the attention based BCI and the number of muscles a human can control promises complex actions that could be performed, the number of different actions that can actually be performed using motor imagery based BCI strongly depends on the way the brain signals are measured and not all limbs are suitable for motor imagery based

BCI. The corresponding areas in the cortex have to be large enough to produce patterns that are distinguishable from the background EEG noise, and sufficiently far away from each other in order to make the ERD/ERS patterns distinguishable from each other. For example, when measuring brain activity using EEG, the ERD/ERS patterns for imagined left- and right hand movements are most prominent over electrode location C3 (right hand), and C4 (left hand). The cortical areas for left- and right foot on the other side, are very close and the corresponding patterns appear both on electrode location Cz. This makes the left- and right foot movements almost indistinguishable from each other using EEG. The comparatively low spatial resolution of EEG is the reason why usually only few (e.g. two or three) different actions can be used with motor imagery based BCI using EEG [36]. However, the risks associated with brain surgery, make invasive BCIs only suitable for a very small set of subjects, mostly patients that would need a brain surgery anyway. Compared to attention based BCI, motor imagery based BCI has a higher error rate and an estimated 15% to 30% of subjects are not able to obtain control using motor imagery based BCI without proper training [37]. Another major limitation for healthy subjects is that one cannot really use motor imagery based BCI while doing something else. As every movement the subject makes creates ERD/ERS patterns, the subject has to avoid any movement in order to use motor imagery based BCI properly.

BCI based on oscillatory activity are BCI that use mental states which lead to changes in the oscillatory components of EEG signals, i.e., that lead to change in the power of EEG signals in some frequency bands. Increase of EEG signal power in a given frequency band is called an Event Related Synchronization (ERS), whereas a decrease of EEG signal power is called an Event Related Desynchronization (ERD) [38]. BCI based on oscillatory activity notably includes motor imagery-based BCI, Steady State Visual Evoked Potentials (SSVEP)-based BCI [39] as well as BCI based on various cognitive imagery tasks such as mental calculation. As an example, imagination of a left hand movement leads to a

contralateral ERD in the motor cortex (i.e., in the right motor cortex for left hand movement) in the μ and β bands during movement imagination, and to an ERS in the β band (beta rebound) just after the movement imagination ends [38].

2.5 Components of an EEG System

In BCI design, EEG signal is used to detect and quantify features of brain signals that indicate the user's intentions and to translate these features into device commands that accomplish the user's intent. To achieve this, a BCI system consists of three sequential stages shown in figure 2.3. The process includes pre-processing, feature extraction and classification.

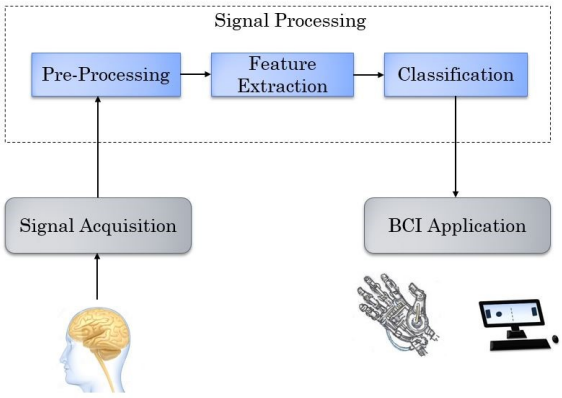

Figure 2.3: Basic design and operation of any BCI system

2.5.1 Preprocessing

2.5.1.1 EEG Artifacts

EEG artifacts exist in recorded signals and are non cerebral in origin. They may be divided into categories: physiological artifacts and non physiological artifacts. Physiological artifacts arise from the variety of body activities that are due to either movement of head,

body and scalp that affect the electrode scalp interface or bioelectric potentials generated with in the body from moving sources like eyes, tongue or stationary sources such as muscles. Nonphysiological artifacts arise from external electric interference from other power sources such as power lines or electric equipment.

EEG signal can be contaminated at many points during the recording and transmission process. EEG signals are known to be very noisy, as they can be easily affected by the electrical activity of the eyes (EOG: Electroocculogram) or of the muscles (EMG: Electromyogram). Most of the artifacts are generated by sources external to the brain. Some common EEG artifacts are as shown in figure 2.4.

- Eye Blink artifact: It is very common in EEG data and produces a high amplitude signal that can be many times greater than EEG signals of interest. Because of its high amplitude, an eye blink can corrupt data on all electrodes, even those at the back of the head. Eye artifacts are often measured more directly in the electrooculargram (EOG) with pairs of electrodes placed above and around the eyes.

- Eye Movement: These artifacts are caused by the reorientation of the retinocorneal dipole [40]. The effect of this artifact is stronger than that of the eye blink artifact. Eye blinks and movements often occur at close intervals.

- Line Noise: Strong signals from A/C power supplies shown in figure 2.4(d) can corrupt EEG data as it is transferred from the scalp electrodes to the recording device. This artifact is often filtered by notch filters, but for lower frequency line noise and harmonics this is often undesirable. If the line noise or harmonics occur in frequency bands of interest, these interfere with EEG that occurs in the same band [41]. Notch filtering at these frequencies can remove useful information. Line noise can corrupt the data from some or all the electrodes depending on the source of the problem.

- Muscle Activity: These artifacts are caused by activity in different muscle groups

such as neck and facial muscles. These signals have a wide frequency range and can be distributed across different sets of electrodes depending on the location of the source muscles.

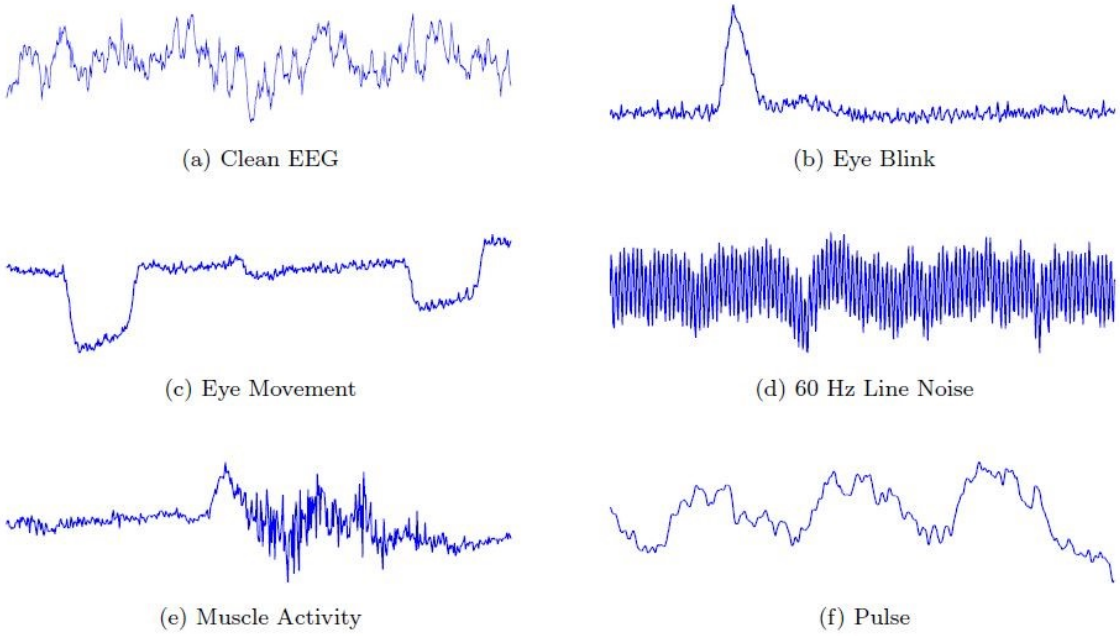

Figure 2.4: Artifacts associated with EEG signal [2]

Artifacts in EEG are commonly handled by discarding the affected segments of EEG. The recognition of the eye blink and eye movement artifacts are generally by a voltage increase in the EOG channel above a threshold, generally 100 μV. Discarding segments of EEG data with artifacts can greatly decrease the amount of data available for analysis. The first attempts at removing artifacts focused on eye blinks. Regression using the EOG channel was attempted in the time and frequency domain [2]. These methods all rely on a clean measure of the artifact signal to be subtracted out. Since the EOG is contaminated with EEG signals, the regression of ocular artifacts has the undesired effect of removing EEG signals from the observations. Regression techniques are the most common type of artifact removal in use [42]. Comparisons of artifact removal using different transformations can

be found in [43]. The artificial mixing matrices were chosen to approximate mixing in the scalp. The common spatial patterns (CSP) technique was used by Koles [44] to remove abnormal components from an EEG recording. The CSP method requires the use of two data sets. No quantitative evaluation was done on the removal but it was visually observed that the artifacts were extracted into a small number of components that would allow their removal. Components are generally selected for removal by visual inspection, but in online filtering systems, artifact recognition is important for achieving the automatic removal of artifact signals. Jung [41] suggests that the spectral structure might be distinct for certain artifact components (e.g., line noise) and that this would allow for automatic removal of these artifacts. Kalman filters and extended Kalman filters have also been used for artifact detection with success depending heavily on the artifact type [45]. This approach was most successful at recognizing EEG signal containing muscle and eye movement artifacts.

2.5.2 Feature Extraction

Feature extraction aims at representing raw or preprocessed EEG signals by an ideally small number of relevant values, which describe the task-relevant information contained in the signals. These features should be selected to minimize the intra-class feature variances while maximizing inter class variances. In other words, their values should be as different as possible between different classes. BCI based on oscillatory activity (e.g., BCI based on ERD/ERS) mostly use spectral and spatial information as features whereas BCI based on event-related potential (ERP) mostly use the temporal and spatial information.

Feature selection are classical algorithms widely used in machine learning [46] and as such also very popular in BCI design [47]. This algorithms evaluate the discriminative (or descriptive) power of each feature individually. The usefulness of each feature is typically assessed using measures such as Student t-statistics, which measures the feature value difference between two classes, correlation based measures such as R^2, mutual information,

which measures the dependence between the feature value and the class label. Uni-variate methods are usually very fast and computationally efficient but they are also sub-optimal. Indeed, since they only consider the individual feature usefulness, they ignore possible redundancies or complementarities between features. As such, the best subset of N features is usually not the N best individual features. As an example, the N best individual features might be highly redundant and measure almost the same information. As such using them together would add very little discriminant power. On the other hand, adding a feature that is individually not very good but which measures a different information from that of the best individual ones is likely to improve the discriminative power much more. These algorithms typically use measures of global performance for the subsets of features, such as measures of classification performances on the training set(typically using cross-validation or multivariate mutual information measures [48]. This global measure of performance enables to actually consider the impact of redundancies or complementarities between features. Some measures also remove the need to manually select the value of N (the number of features to keep), the best value of N being the number of features in the best subset identified. However, evaluating the usefulness of subsets of features leads to very high computational requirements. Indeed, there are many more possible subsets of any size than individual features. As such there are many more evaluations to perform. In fact, the number of possible subsets to evaluate is very often far too high to actually perform all the evaluations in practice. Consequently, multivariate methods usually rely on heuristics solutions in order to reduce the number of subsets to evaluate. Multivariate methods are also suboptimal but usually give much better performances than univariate methods in practice.

2.5.2.1 Optimal Feature Extraction

To extract the most relevant information from the EEG signal Pharino [49] introduced r square correlation coefficient for the best frequency and time parameter. Optimum R-square

coefficient gives the active frequency band and specific channel that is strongly correlated with the action performed. In [50], the study had showed that spectral component of brain activation related to motor imagery task using ERD was found in μ band(10-12 Hz) and using ERS was found in β band (13 to 30 Hz), but they varied from subject to subject significantly. To get the optimal features over that frequency band, frequency selection method like in [51] for subject specific frequency band need to be searched and selected independently from each subject. In [52], spatial information had been considered. Even though neurophysiology confirms that the most significant channel location related to motor imagery are C3, C4 and Cz, the EEG signals are spread over the area around these electrodes. In different experiments with different subjects, the distributions of EEG signals over the location are different. To adapt BCI system over a wide range of subjects, the spatial-spectral-temporal parameter of EEG signals need to be searched and tuned before using in the system. In [53] spatio-spectral and temporal parameter searching algorithm using class correlation and particle swarm was optimization was proposed. This proposed method composed of series of parameter searches in order of channels, time and frequency bands of EEG. This process showed rejection concept of the focus ERD/ surrounded ERS which can be used in motor imagery tasks. But it showed the promising result and confirmed that these specific parameters need to be analyzed for real-life BCI applications. In [54], author proposed using genetic algorithm (GA) for automatic feature extraction in P300 detection. The variation of coding the information of gene in a chromosome and natural selection of GA could be used in search algorithm for optimal features based on the spatio-spectral-temporal parameters.

2.5.2.2 Common Spatial Pattern

Common Spatial Pattern [12] method was employed as one of the techniques for feature extraction in the present study. Details of the algorithm are described in section 3.4.2.

The filtered signal corresponding to the desynchronization of the left-hand motor cortex is characterized by a strong motor rhythm during imagination of right hand movements, and by an attenuated motor rhythm during left hand imagination. This criterion is exactly what the CSP algorithm optimizes: maximizing variance for the class of right hand trials and at the same time minimizing variance for left hand trials.

2.5.2.3 Empirical Mode Decomposition (EMD) and Its Variants

More recently a technique, termed Hilbert-Huang transform (HHT) [9], for analyzing nonlinear and non-stationary signals, has been utilized to analyze biomedical signals. Application of the HHT algorithm for discrimination of mental tasks is proposed in this research. As an algorithm of time-frequency analysis, HHT can produce physically meaningful representations of signal both in time and frequency domains. The core of this algorithm to decompose signal is data dependent and posteriori-defined, and the inner scales of the decomposed signal are adapted for EEG signal processing. HHT is composed of empirical mode decomposition (EMD) and Hilbert spectral analysis (HSA), which intuitively decomposes original signal into a set of symmetric intrinsic mode functions (IMFs) that are amplitude and frequency modulated [55]. It has been widely used for analyzing non-stationary signals. Moreover, this technique is a useful tool for quantifying the global regularity of EEG signal [56, 57] and spectral entropy and spectral energy of IMFs were used to automatically diagnose seizure. The prediction and detection of seizure were done with continuous wavelet entropy from EEG signals.

EMD is a nonparametric and self-adaptive method that decomposes any signal to a get finite number of functions called intrinsic mode functions (IMFs) [9]. EMD does not require any predefined basis function to represent the signal, which is the advantage of EMD over Fourier and wavelet analysis. This algorithm has advantages in biomedical applications. In [58] EMD has been combined with chaos analysis to recognize the chaotic properties

of ECG signals. EMD is also used to extract features from ECG signals during cardiac auscultation using morphological signal processing [59]. In [10], Wu proposed Ensemble Empirical Mode Decomposition (EEMD) to improve the accuracy of measurements where a white noise is added to the targeted data. According to [60] EEMD is a truly noise-assisted data analysis (NADA) method and represents a substantial improvement over the original EMD. A combination of EEMD-ICA EEMD-ICA algorithm is successfully applied in [61] to separate the recorded signals to independent components to remove the artifacts. An extension of EMD called multivariate empirical mode decomposition (MEMD) is proposed in [11] which showed the direct multi-channel signal processing using localization of frequency information. A combination of CSP and EMD method is proposed in [62] where third order temporal moments, and spectral features including spectral centroid, coefficient of variation and the spectral skew of the IMFs are used for feature extraction from EEG signals. Besides the strengths of feature extraction methods related to instantaneous frequencies (IF), it is important to note that the extraction of IF is more meaningful when the IMFs extracted from the EEG signals are mono component [63].

2.5.3 Classification

EEG signals are generally represented in high dimensional feature space and it is very difficult to interpret manually. Machine learning methods are helpful for interpreting high dimensional feature sets and analyze the characteristics of brain signal patterns. According to [3] classifiers used in BCI research are generally of 5 types. Linear classifiers, nonlinear classifiers, neural network, nearest neighbor classifiers and a combination of these.

Linear classifiers are discriminant algorithms that use linear functions to distinguish classes. These are the most popular algorithms for BCI applications. Neural network is also a widely used classifier in BCI research. Neural network is an assembly of several artificial neurons which enable to produce nonlinear decision boundaries. Non linear classifiers pro-

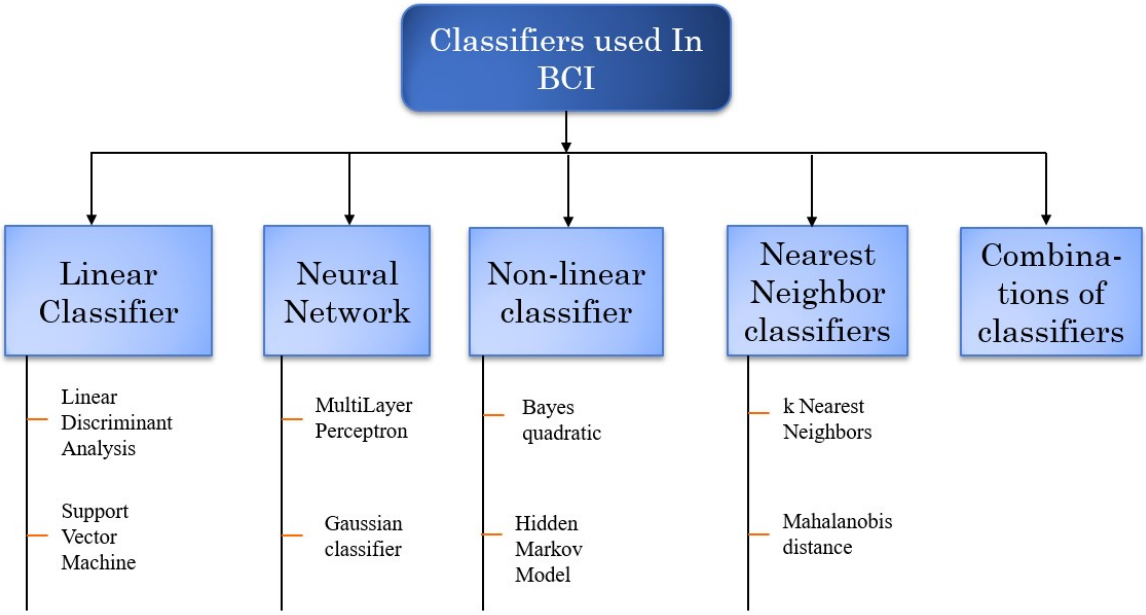

Figure 2.5: Different types of Classifiers used in BCI

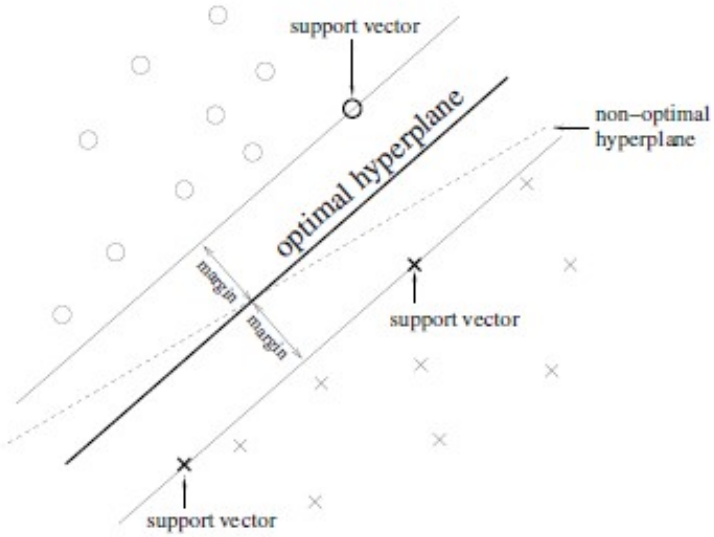

Figure 2.6: SVM finds the optimal hyperplane for generalization [3].

duce nonlinear decision boundaries which enable them to perform more efficient rejection of uncertain samples than discriminative classifiers. However, these classifiers are not as widespread as linear classifiers or neural networks in BCI applications[59].

One of the most used linear classifiers is support vector machine (SVM). SVM gave the best results in several synchronous experiments, in its linear [64] or nonlinear form [65], in binary or multiclass BCI. Regularized Fisher's LDA shares several properties with SVM such as being a linear and regularized classifier. LDA technique has a very low computational requirement which makes it suitable for online BCI system. Moreover this classifier is simple to use and generally provides good results. Consequently, LDA has been used with success in a great number of BCI systems such as motor imagery based BCI [38]. Its training algorithm is even very close to the SVM one. Consequently, it also reached very interesting results in some experiments [66]. The first reason for this success may be regularization. Actually, BCI features are often noisy and likely to contain outliers. Regularization may overcome this problem and increase the generalization capabilities of the classifier. As a consequence, regularized classifiers, and more particularly linear SVM, have outperformed unregularized ones of the same kind, i.e., LDA, in several BCI studies. Similarly a nonlinear SVM has outperformed an unregularized nonlinear classifier, namely, an multi layer perceptron (MLP), in another BCI study [47].

CHAPTER 3

METHODOLOGY

The details of methodology used in this work are presented in this chapter. First the EEG system along with its hardware and software components is discussed. Next the details of data acquisition system are presented. It is followed with presentation of signal processing algorithms used in this work for artifact removal form acquired EEG signals. Next feature selection algorithms are discussed along with extraction of features from pre-processed EEG signals. Finally, classification technique for identification of actual and MI activities using extracted features is presented.

3.1 EEG System

The EEG system features sixty four electrodes across the central nodes according to figure 3.1 placed against the head using an EEG cap. This placement is based on the 10/20 64 electrode system using a referential montage. A conductive gel is used as a medium between the electrodes and the scalp to reduce the effects of skin impedance. Electrodes are attached to the earlobe to provide a reference voltage. Finally, the ends of these leads are plugged into the SynAmps RT amplifier shown in figure 3.2(d).

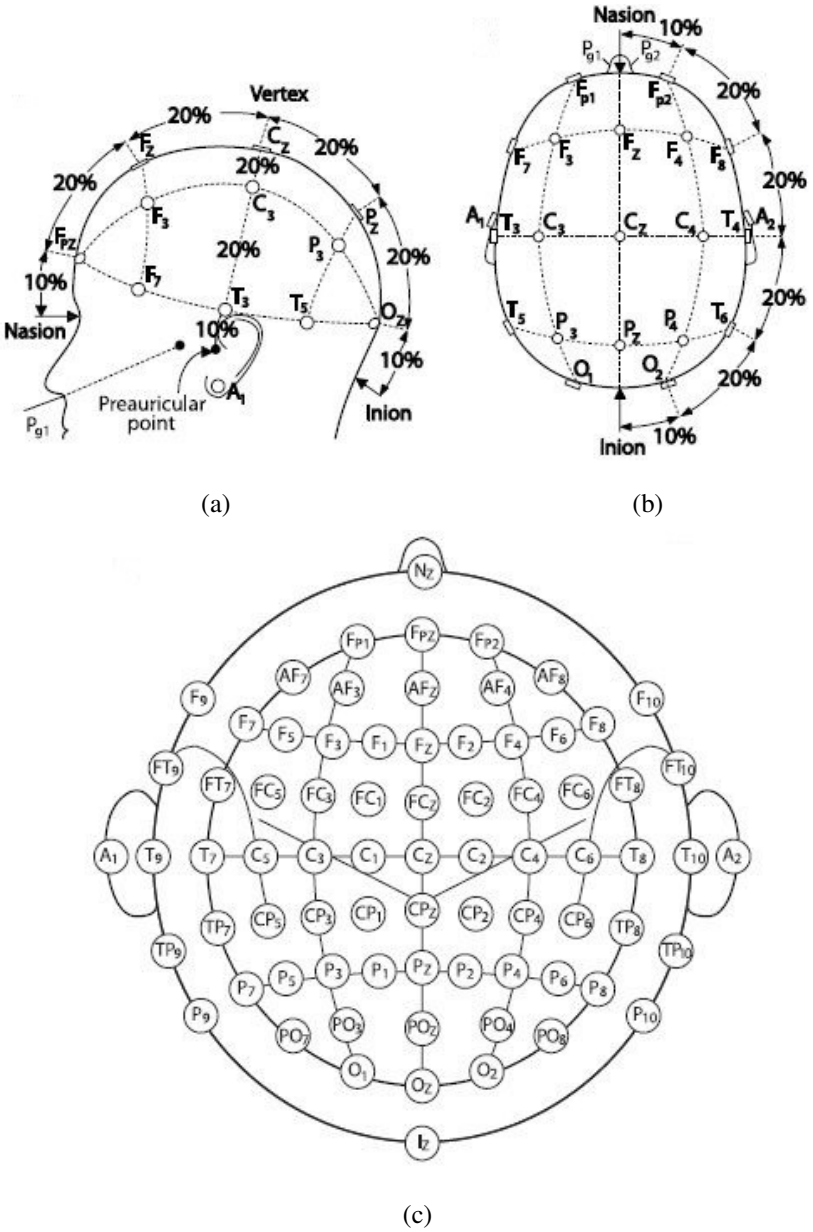

Figure 3.1: International 10-20 system for electrode placement [4]

The electrodes are placed according to this system with the inactive or common electrode at a remote location of the skull (earlobe, nose, or chin). It is denoted as nasion and inion. Ten percent of the data points are on prefrontal and occipital planes. The rest is divided in four parts.

Table 3.1: Cross sectional planes in international 10-20 system

Cross-sectional Planes	Notation
Prefrontal	Fpz
Frontal	Fz
Vertex	Cz
Parietal	pz
Occipital	Oz

3.1.1 Hardware

3.1.1.1 Electrodes

Sintered silver/silver chloride (Ag/AgCl) electrodes are used in brain cap which are made from very finely powdered high purity silver and silver chloride. These are mixed in a specific ratio and compacted into the electrode body at very high pressure. The resulting pellet is relatively thick (0.7mm to 1.0mm) and never needs to be rechloridized because it is a homogeneous mixture.

3.1.1.2 Skin preparation kits

Most amplifiers are designed to allow recordings from high impedance electrodes, but with a potentially significant reduction in data quality due to radiated electrical noise. Conductivity gel makes the impedance value below threshold and the skin preparation gel makes the scalp ready for use of conductivity gel through the electrodes. This facilitates parting the hair and preparing the scalp to obtain the lowest possible impedance, without direct skin abrasion.

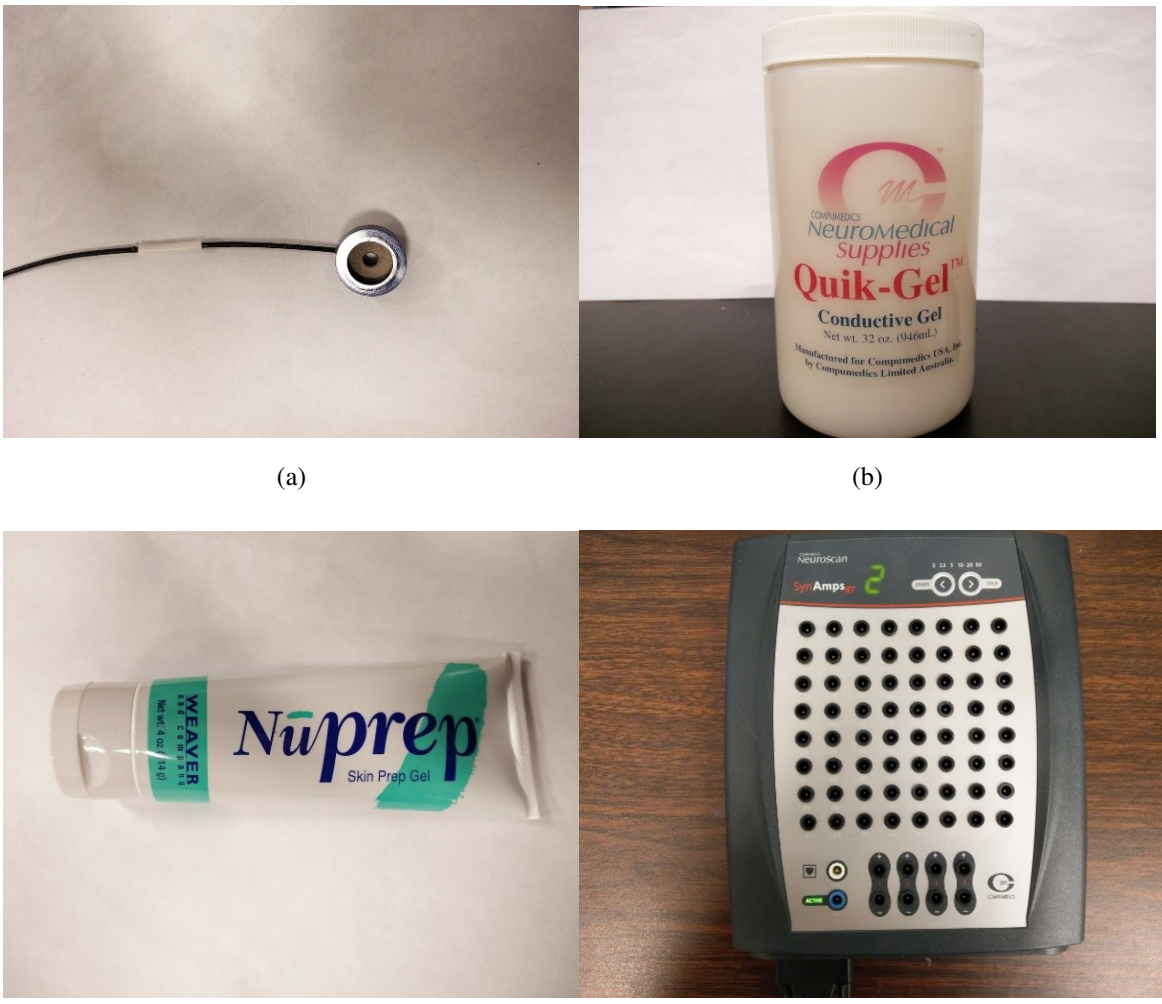

(a) (b)

(c) (d)

Figure 3.2: Data Acquisition accessories (a) Electrode (b) Conductive gel (c) Skin preparation gel and (d) SynAmps RT Amplifier

3.1.1.3 Amplifier

SynAmps RT is the one of the latest EEG, ERP and EP amplifier from Compumedics Neuroscan. Using the most current technology, the RT builds on the quality of the past SynAmps series of amplifiers and extends the specifications beyond anything that has come before. SynAmps RT sets a new standard in amplifier technology, providing a system

suitable for recording everything from high sampling rate (20,000 Hz) Auditory Brain Stem recordings. The technical specification of SynAmps RT amplifier is given as follows:

- A USB 2.0 interface is used to link the SynAmps RT and computer. This single connection serves up to four headboxes for a total of 256 EEG channels (plus additional bipolar and HLI channels) via a single system unit. A second system unit can be used for more channels (depending on the computer's speed and the AD rate).
- Real-time digital filtering provides a wide range of filter settings from DC to 3.5 kHz.
- Sampling rates up to 20 kHz from 1 to 64 EEG channels on a single headbox. Sampling rate is independent of the number of headboxes attached to a system.
- It supports 64 monopolar, 4 bipolar, and 2 high-level input channels. A high density connector on the headbox is provided for quick connection to electrode cap arrays.
- 24-bit AD conversion provides greater resolution and the impedance measurement 1KΩ to 200 KΩ.

3.1.2 Software

3.1.2.1 BCI2000

BCI2000 is a software suite for brain-computer interface research. It is commonly used for data acquisition, stimulus presentation, and brain monitoring applications. BCI2000 supports a variety of data acquisition systems, brain signals, and study/feedback paradigms. During operation, BCI2000 stores data in a common format (BCI2000 native or GDF), along with all relevant event markers and information about system configuration. BCI2000 also includes several tools for data import/conversion, a routine to load BCI2000 data files directly into Matlab and export facilities into ASCII.

BCI2000 is based on a model that can describe any BCI system and that is similar to the one described in [67]. This model shown in figure 3.3, consists of four modules that communicate with each other: Source (Data Acquisition and Storage), Signal Processing, User Application, and Operator Interface. The modules are separate programs that communicate through a TCP/IP-based protocol. This protocol can transmit all information needed for operation. Thus, the protocol does not need to be changed when changes are made in a module.

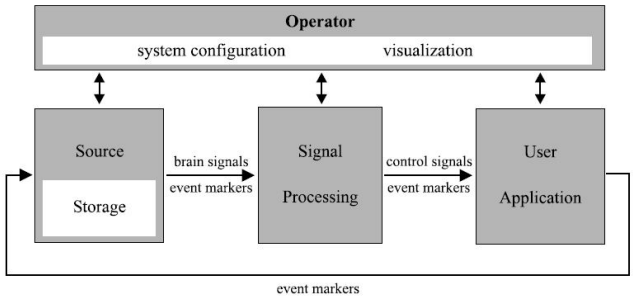

Figure 3.3: Four modules of BCI2000

The Source module acquires brain signals and passes calibrated signal samples on to the Signal Processing module. The Source module consists of a data acquisition component, and a data storage component that implements the native BCI2000 file format, as well as EDF, which is a data format popular in sleep research [68], and GDF, a variant of EDF designed for BCI applications [69]. The data acquisition component has a number of implementations. The BCI2000 file format consists of an ASCII header that defines all parameters used for this particular experimental session, followed by binary signal sample and event marker values. It supports 16- and 32-bit integer formats as well as a 32-bit floating point format. The BCI2000 distribution includes Matlab MEX files for manipulating BCI2000 data files, and for other tasks. MEX files allow the execution of externally compiled code from within Matlab. BCI2000 MEX allows for convenient access to BCI2000 data files or functions directly from Matlab.

3.2 Data Acquisition

EEG signal is collected with BCI2000. During the data acquisition session, the screen will either be blank, or display an instruction, such as Right Hand, Left Hand, Both Hands, or Both Feet. The instruction will appear on the screen for 3 seconds; during this time, the subject should continuously imagine the movement shown in figure 3.4. The hand movements should be opening and closing the hands, and the foot movement should be moving the feet back and forth. When the screen is blank, the body should be completely relaxed.

During a run, each body part movement (actual or imagined) is repeated 20 times. Ideally, there should be 100 data points, meaning that there should be a total of 5 runs. With multiple sessions, fewer runs are necessary, since the subject is able to perform the task better. The experiment data were sampled at 256 Hz.

Figure 3.4: Photographs during the process of acquisition of EEG signal acquisition

Three different subjects are used to record the EEG signal. Two of them are right handed and another one is left handed. All the subjects are in between 24 to 27 years old.

Table 3.2: Subject's description

Subject	Gender	Age	Preferred hand
1	M	26	Left
2	M	27	Right
3	M	24	Right

3.3 Signal Processing Algorithms

3.3.1 Independent Component Analysis

Independent component analysis is one of a group of algorithms to solve the problem of blind source separation.

The observed signal is denoted by x with elements x_1 , ..., x_n, the source is denoted by s with elements s_1, ..., s_n and A is the mixing matrix a_{ij}. With the vector notation, mixing models can be written as equation 3.1 [70]

$$x = As \tag{3.1}$$

Estimating the independent components can be accomplished by finding the right linear combinations of the mixture variables, with matrix inversion, as

$$s = A^{-1}x \tag{3.2}$$

thus, to estimate one of the independent components, we can consider a linear combination of the x_i. Assuming a new vector

$$y = b^T x = \sum_{i=1}^{n} b_i x_i \tag{3.3}$$

where b is a vector to be determined. by substituting equation 3.1 to equation 3.3 it can be written $y = b^T As$.Thus, y is a certain linear combination of the s_i, where b^T A is a

coefficient matrix denoted by q. So obtained in equation 3.4

$$y = b^T x = q^T s = \sum_{i=1}^{n} q_i s_i \tag{3.4}$$

if b were one of the rows of the inverse of A, this linear combination $b^T x$ would actually be equal one of the independent components. In that case, the corresponding q would be such that just one of its elements is 1 and all the others are zero. In practice b and A cannot be determined directly, but can be found with an estimator that gives a good approximation. The fundamental idea here is that since a sum of even two independent random variables is more Gaussian than the original variables, $y = q^T s$ is usually more Gaussian than any of the s_i and becomes least Gaussian when it in fact equals one of the s_i. In this case, obviously only one of the elements q_i of q is nonzero. In practice the values of q is unknown, but $q^T s = b^T x$ by the definition of q. Such a vector would necessarily correspond to a $q = A^T b$, which has only one nonzero component. This means that $y = b^T x = q^T s$ equals one of the independent components.

3.3.2 Empirical Mode Decomposition (EMD)

Empirical Mode Decomposition (EMD) is a way of decomposing signals to get a finite number of functions called intrinsic mode functions (IMFs). It is designed to work well for signals that are nonstationary and nonlinear. In contrast to other common transforms like the Fourier transform, the HHT is more like an algorithm (an empirical approach) that can be applied to a data set, rather than a theoretical tool. The process of EMD is presented briefly for completeness [71, 72].

For a given signal, x(t), local highest and lowest points are found as a first step of EMD. A cubic spline curve is used to connect all the local highest and lowest points (extrema) giving upper envelope $x_u(t)$ and low envelope $x_l(t)$. Further, to observe the values at every point of envelopes the mean value curve is calculated. The mean value, $m_1(t)$ is defined as

equation 3.5 for two envelopes

$$m_1(t) = \frac{x_u(t) + x_l(t)}{2} \tag{3.5}$$

In this way, the value for the first IMF, $h_1(t)$ can be calculated using equation 3.6

$$h_1(t) = x(t) - m_1(t) \tag{3.6}$$

The process of obtaining the IMF is generally known as shifting process. This process is used to cut off the riding waves and to ensure the symmetry of wave-profiles. It is a recurring process. For this, during the next shifting process $h_1(t)$ is considered as original data and the notation for second IMF is as follows:

$$h_{11}(t) = h_1(t) - m_{11}(t) \tag{3.7}$$

The shifting process is repeatable for k times. It is continued till $h_1k(t)$ is considered as an IMF.

$$h_{1k}(t) = h_{1(k-1)}(t) - m_{1k}(t) \tag{3.8}$$

The relation between first IMF $c_1(t)$ and $h_{1k}(t)$ can be defined as follows:

$$c_1(t) = h_{1k}(t) \tag{3.9}$$

Furthermore, it is mandatory to use some stopping criteria to end the shifting process so that it can ensure the continuity of sufficient physical sense of both amplitude and frequency modulations of IMF elements. The size of standard deviation (SD) is the stopping criteria and can be designated as equation 3.10

$$SD = \sum_{t=0}^{T} \frac{\mid h_{k-1}(t) - h_k(t) \mid^2}{h_{k-1}^2} \tag{3.10}$$

The first IMF $c_1(t)$ is achieved for the smaller value of SD compared to threshold value. The value of residue is computed using the following equation 3.11

$$r_n(t) = x(t) - \sum_{i=1}^{n} c_i(t) \tag{3.11}$$

The following flow chart shown in figure 3.5 can briefly explain the whole method:

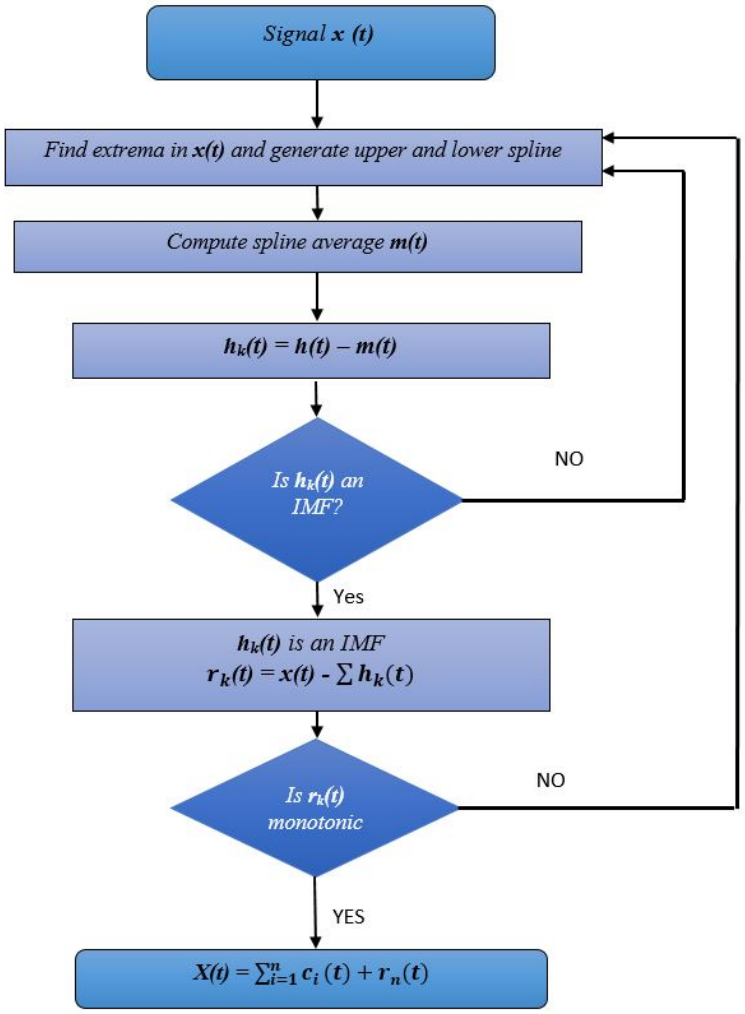

Figure 3.5: Flow chart of Empirical Mode Decomposition algorithm

EMD Steps involved in the algorithm are:

1. Collection of EEG signals with significant amount of artifacts.

2. Perform Empirical Mode Decomposition over the data to obtain the set of intrinsic mode functions (IMFs).

3. Calculate the feature value of each of the IMF.

4. Identify the different levels of IMF in which the feature value increases or decreases rapidly from a small value.

5. Reconstruct the signal by the avoidance of those IMFs to get the corrected signal.

3.3.3 Ensemble Empirical Mode Decomposition

EMD approach has a drawback called mode mixing that happens when different IMFs have similar scale. Mode mixing is one of the major weaknesses of EMD. To overcome this problem Wu and Huang [10] proposed a new algorithm called Ensemble Empirical Mode Decomposition (EEMD).

The basic steps for EEMD algorithm are as follows:

1. Initialize the number of ensemble I,
2. Generate $x_i(t) = x(t) + w_i(t), (i = 1, ...I)$ are different realization of Gaussian noise
3. Each $x_i(t)$ is fully decomposed by EMD getting their modes $IMF_k^i(t)$,
4. Assign $\overline{IMF}$ as the k-th mode of x(t), obtained as the average of the corresponding $IMF_k^i : \overline{IMF}_k(t) = \frac{1}{I}\sum_{i=1}^{I} IMF_k^i(t)$

x(t) can be reconstructed according the following equation 3.12:

$$x(t) = \sum_{k=1}^{K} \overline{IMF}_k(t) + \bar{r}(t) \tag{3.12}$$

3.3.4 Multivariate Empirical Mode Decomposition

To ensure the complete removal of the white noise, multivariate empirical mode decomposition is used. The following algorithm proposed in [11] is employed here to decompose signal x(t) into a set of IMF components.

1. Generate the point-set for sampling on an $(n-1)$-sphere
2. Calculate a projection, $\{p^{\theta_k}(t)\}_{t=1}^{T}$ of the input signal $\{x(t)\}_{t=1}^{T}$ along the direction vector A^{θ_k}, for all k (the whole set of direction vectors), giving $\{p^{\theta_k}(t)\}_{k=1}^{K}$ as the set of projections

3. Find the time instants $\{t_i^{\theta_k}\}_{k=1}^{K}$ corresponding to the maxima of the set of projected signals $\{p^{\theta_k}(t)\}_{k=1}^{K}$

4. Interpolate $[t_i^{\theta_k}, x(t_i^{\theta^k})]$, for all values of k, to obtain multivariate envelope curves $\{e^{\theta_k}(t)\}_{k=1}^{K}$;

5. For a set of K direction vectors, calculate the mean $\mu(t)$ of the envelope curves as:

$$\mu(t) = \frac{1}{k}\sum_{k=1}^{K} e^{\theta_k}(t) \tag{3.13}$$

6. Extract the detail $d(t)$ using $d(t) = X(t) - \mu(t)$. If the detail $d(t)$ fulfills the stoppage criterion for a multivariate IMF, apply the above procedure to $X(t) - d(t)$, otherwise apply it to $d(t)$.

3.3.5 Performance Evaluation

Differential amplifiers with band-pass filters are used to minimize the effects of high frequency noise and low frequency artifacts. By selecting channels of each segment as pure EEG, the pure EEG signals were stored in the matrix A (6 X 1600). The EMG artifact was generated by using random noise band-pass filtered between 20 and 60 Hz in Matlab, and the muscle artifacts were stored in the matrix B (6 X 1600). The noise-contaminated EEG signal can be obtained by mixing the matrix A with the matrix B in the following equation 3.14

$$C(i) = A(i) + \lambda * B(i), i = 1, 2, ..., n \tag{3.14}$$

The SNR of signals can be defined (in dB) as following equation 3.15

$$SNR = 10 * log(\frac{\sum_{i=1}^{n} x_i^2}{\sum_{i=1}^{n} y_i^2}) \tag{3.15}$$

Where x_i denote the pure EEG signals, y_i represent the artifacts and n is the total number of samples before the artifact removal. After getting rid of the artifacts, x_i denotes the pure

EEG signal and y_i is calculated by subtracting artifact-free EEG signal from the raw EEG signal.

The MSE indicates the degree of similarity of the two signals. The smaller the value of MSE is, the higher the degree of similarity between two signals is. The MSE of signals can be calculated using equation 3.16

$$MSE = \frac{1}{n}\sum_{i=1}^{n}(x_i - y_i)^2 \tag{3.16}$$

where x_i denote the pure EEG signals and y_i represent the mixed EEG signals. Therefore, the MSE can be used to depict the degree of EEG information after performing the artifact removal.

3.4 Feature Selection Algorithm

3.4.1 R square Coefficient Method

The Fourier transform depicts the similarity between a signal and a sinusoidal with a single complex number. The magnitude of the complex number captures the degree to which oscillations at a particular frequency contribute to the signal's energy, while the argument of the complex number captures phase information. Short-time Fourier transform (STFT) is a technique applying a chosen time function or window to the input signal and calculate the Fourier transform. According to [44] the mathematical properties describe by the equation 3.17 . x(t) is the input signal and ω(t) is the window function and X(ω , t) is the transformed signal as a function of normalized frequency and time .

$$X(\omega, \tau) = \int x(t)\omega(t-\tau)e^{-j\omega t}dt \tag{3.17}$$

R-square coefficient is a square of Pearson correlation coefficient of two random samples x_i and y_i. It is given in equation 3.18. $\bar{x}$, $\bar{y}$ are means of sample x and y, n is total number

of sample. In this work sample xi and yi are STFT samples from channel C3 and C4 of the EEG signal. R_t^2 component related to time component and R_f^2 component related to frequency component are found.

$$R^2 = \frac{(\sum x_i y_i - n\bar{x}\bar{y})^2}{(\sum x_i^2 - n\bar{x}^2)(\sum y_i^2 - n\bar{y}^2)} \tag{3.18}$$

To obtain optimal frequency parameter of separation between signals from each class, the value of frequency as in equation 3.19 is selected.

$$f_{optimal} = arg_f max(R_f) \tag{3.19}$$

While the optimal temporal parameter is chosen by equation 3.20 and the total ranges around the optimal value $t_{optimal}$ is selected as in equation 3.21.

$$t_{optimal} = arg_t max(R_t) \tag{3.20}$$

$$T_{optimal} = [t_{optimal} - 0.25t_{optimal} + 0.025] \tag{3.21}$$

After optimal spectral parameter $f_{optimal}$ and temporal parameter $T_{optimal}$ have been found, these are used to select the optimal time-frequency pairs from both channels C3 and C4. The complete flow chart for feature extraction based on R-square coefficient is shown in figure 3.6

3.4.2 Common Spatial Pattern

Common Spatial Pattern method was employed for feature extraction in this study. Details of the algorithm are described in the following with the example of discriminating left hand vs. right hand imagery (MI). The filtered signal corresponding to the desynchronization of the left hand motor cortex is characterized by a strong motor rhythm during imagination of right hand movements, and by an attenuated motor rhythm during left hand imagination. This criterion is exactly what the CSP algorithm optimizes: maximizing variance for the class of right hand trials and at the same time minimizing variance for left hand trials.

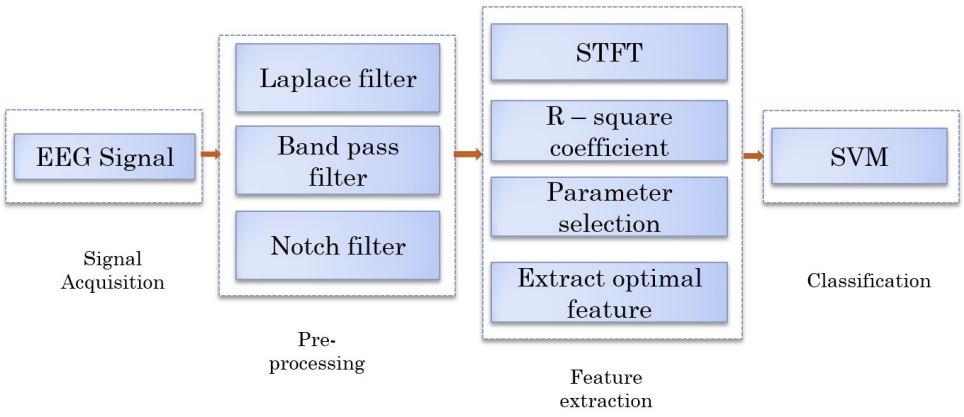

Figure 3.6: Optimal feature extraction based on R-square coefficient method

Details of the algorithm are described as follows with the example of classifying single-trial EEG during right hand and left hand movements [12]. X_R and X_F denote the preprocessed EEG matrices under two conditions (hand and foot) with dimensions $N \times T$, where N is the number of channels and T is the number of samples per channel. The normalized spatial covariance of the EEG can be represented as equations 3.22 and 3.23

$$C_R = \frac{X_R X_R^T}{trace(X_R X_R^T)} \tag{3.22}$$

$$C_L = \frac{X_L X_L^T}{trace(X_L X_L^T)} \tag{3.23}$$

X^T is the transpose of X and trace(X) computes the sum of the diagonal elements of X. The averaged normalized covariance C_R and C_L are calculated by averaging over all the trials of each group. The composite spatial covariance can be factorized as equation 3.24

$$C = C_r + C_L = U_o \Psi U_o^T \tag{3.24}$$

Where Uo is the matrix of eigenvectors and Ψ is the diagonal matrix of eigenvalues. The transformation matrix can be written as equation 3.25

$$P = \Psi^{-\frac{1}{2}} U_o^T \tag{3.25}$$

The matrix P transforms the covariance matrices as

$$C_R{}' = PC_RP^T \tag{3.26}$$

$$C_L{}' = PC_LP^T \tag{3.27}$$

C_R' and C_L' are common eigenvectors and the sum of corresponding eigenvalues for the two matrices will always be one,

$$C_R{}' = U\Psi_RU^T \tag{3.28}$$

$$C_L{}' = U\Psi_LU^T \tag{3.29}$$

$$C_R{}' + C_L{}' = I \tag{3.30}$$

Here I is the identity matrix. The eigenvector with the largest eigenvalues for C_R' have the smallest eigenvalue for C_L' and vice versa. The transformation of EEG onto the eigenvectors corresponding to the largest eigenvalues are optimal for separating variance in two signal matrices. The projection matrix W is denoted as equation 3.31

$$W = U^TP \tag{3.31}$$

With the projection matrix W, the original EEG can be transformed into uncorrelated components

$$Z = WX \tag{3.32}$$

Z can be seen as EEG source component including common and specific components of different tasks. The original EEG X can be reconstructed using equation 3.33

$$X = W^{-1}Z \tag{3.33}$$

3.4.3 Sample Entropy

Sample entropy is explored as a feature in order to discriminate motor task EEG signals. The sample entropy of the signal is defined as the negative natural logarithm of the conditional

probability that two sequences similar for m points remain similar at the next point, where self matches are not included in calculating the probability. Thus, a lower value of sample entropy of the signal also indicates more self-similarity in the time series. For computing the sample entropy of the signal, the embedding dimension (m) and tolerance parameter (r) must be specified [67].

Considering a signal (EEG signal or IMF) x[n] of length N, this signal can be represented by the sequence as, $x[1]; x[2]; ....., x[N]$. m dimension vectors are formed consecutively, starting with the i^th point of the signal sequence

$$X_m(i) = [x(i), x(i+1), ..., x(i+m-1)], i = 1, 2, ...N - m + 1 \tag{3.34}$$

Distance d $(X_m(i), X_m(j))$ is defined between two vectors $X_m(i)$ and $X_m(j)$ as the absolute maximum difference between their scalar components according to equation 3.35 :

$$d(X_m(i), X_m(j)) = \underset{k=0,1,...,m-1}{Max} (\mid x(i+k) - x(j+k) \mid), i \neq j \tag{3.35}$$

For a given tolerance parameter r, for every ith value, compute the distance d$(X_m(i), X_m(j))$ is computed, the number of distances, which are less than or equal to r, are counted and denoted as A_i. Then the ratio of this number to N-m-1, is computed and denoted as $A_i^m(r)$ in equation 3.36 .

$$A_i^m(r) = \frac{1}{N-m-1} A_i \tag{3.36}$$

Then

$$A^m(r) = \frac{1}{N-m} \sum_{i=1}^{N-m} A_i^m(r) \tag{3.37}$$

Dimension is increased from m to m +1, and the steps (1) to (4) are repeated, and $A_i^{(m+1)}(r)$ is computed. Theoretically, sample entropy of signal can be defined as equation 3.38:

$$SampEn(N, m, r) = -ln[\frac{A^{m+1}(r)}{A^m(r)}] \tag{3.38}$$

3.4.4 Band Power

In event related BCI, the time course is directly related to the average of power samples across trials. The band power (BP) is estimated by using the digitally band pass filtered signals and squaring each signal and averaging over consecutive sample according to the given window length. According to [31], band power could be calculated following these steps:

- squaring the amplitude of samples, $X_f(i, j)$, to obtain power samples;
- averaging of power samples across all trials, j = 1, 2, 3, ..., N;
- averaging over time samples to smooth the data and reduce the variability.

Band power can be calculated using the following equation:

$$\bar{p}_i = \frac{1}{N} \sum_{j=1}^{N} x_f(i, j)^2 \tag{3.39}$$

where $\bar{p}_i$ is the band power for sample i of the data set.

3.5 Classification

3.5.1 Support Vector Machine

SVM is used to construct the optimal hyperplane with largest margin for separating data between two groups. For two-dimensional data, single hyperplane is enough to separate the data into two groups such as +1 or -1. Two hyperplanes are needed to separate the data points for three-dimensional data according to figure 3.7.

SVM constructs hyperplane for separating the sample data based on the target categories. For two dimensional data, there are number of possible linear separators (hyperplanes) and it is necessary to find the optimal hyperplane which has maximum margin

width. The lines H1 and H2 are drawn parallel to optimal hyperplane (solid line) and mark the distance between the hyperplane and the data points. The distance between the dotted lines (AC) is called as margin. Some of the sample data points that lie on the hyperplane H1 and H2, are called as Support Vectors (SVs) refer to figure 3.7. These SVs are essential for calculating the margin width. According to [73] linearly separable classification separates the high dimensional data into two groups, y_i=+1,-1 without any overlapping or misclassification. Hyperplanes H1 and H2 are represented as equations 3.40 and 3.41,

$$w_1 x_1 + w_2 x_2 - b = 1 \tag{3.40}$$

$$w_1 x_1 + w_2 x_2 - b = -1 \tag{3.41}$$

where w_1,w_2 are positions of the hyperplane H1 and H2 respectively.x_1,x_2 are data points and takes value of +1,0,-1 which shows how far hyperplanes are away from the original line.The maximum margin width is $\frac{2}{w}$and the minimum margin width is $\frac{1}{2}w$

$$y_i(w_1 x_{i1} + w_2 x_{i2} - b) \geqslant 1, for i = 1, 2, ...m \tag{3.42}$$

Lagrangian multiplier can be denoted as equation 3.43

$$L(w, b, \alpha) = [\frac{1}{2}w^2 - \sum_{i=1}^{n} \alpha_i [y_i w' x_i + b] - 1] \tag{3.43}$$

This implies that,

$$w = \sum_{i=1}^{n} \alpha_i y_i x_i \tag{3.44}$$

Finally, optimal decision function of a classifier is defined as equation 3.45

$$f(y) = sign(\sum_{i=1}^{sv} \alpha_i y_i (x_i x_s v) + b) \tag{3.45}$$

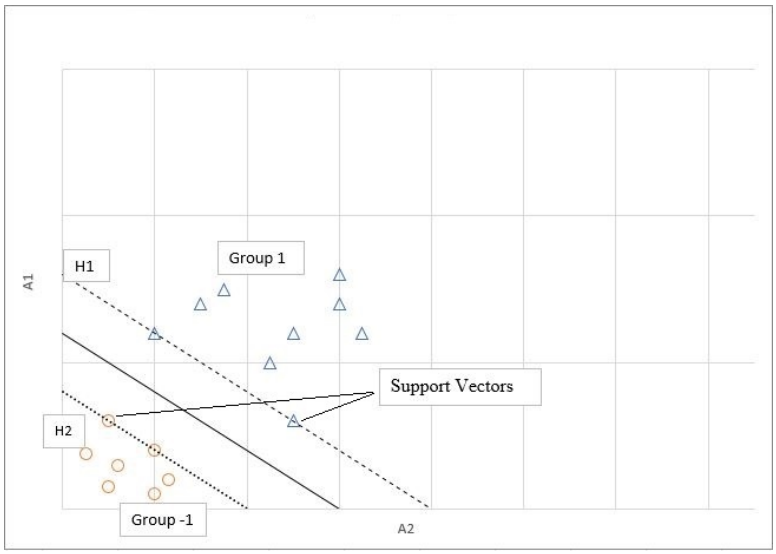

Figure 3.7: Linearly separable SVM technique

CHAPTER 4

RESULTS AND DISCUSSION

Results and discussions are presented in this chapter. The acquired EEG signals for different motor activities are presented first. Next identification of artifacts in EEG signals and removal of artifacts are presented using the signal processing techniques of EMD and the extensions, EEMD and MEMD. It is followed with presentation of performance results of signal to noise ratio (SNR) and mean square error (MSE) for the signal processing algorithms based on EMD and CSP. Next results of extraction of features like r square coefficient, spectral power, band power and sample entropy are presented. Finally, results of identification and classification accuracy of the actual and the imagined motor tasks are presented.

4.1 Acquired EEG Signals

EEG signals were recorded with BCI2000 for different actual and imagined movements. A representative group of EEG signals from several channels is shown in figure 4.1. During the session, the subject was asked to follow the instruction shown in the screen. The instructions were either blank, or displayed an instruction, such as Right Hand, Left Hand, Both Hands, or Both Feet. The instruction appeared on the screen for 3s. During a run, movement (actual or imagined) of each body part was repeated 20 times. There were 100 data sets, for a total of 5 runs for each case. EEG signals were sampled at 256 Hz.

4.2 Artifact Removal

Power spectra of acquired EEG signals were analyzed to look for artifacts. Power spectra of some representative acquired EEG signals form some of the channels are shown in figure 4.1 for subject 1. From these spectra, it is clear that EEG recordings of some channels such

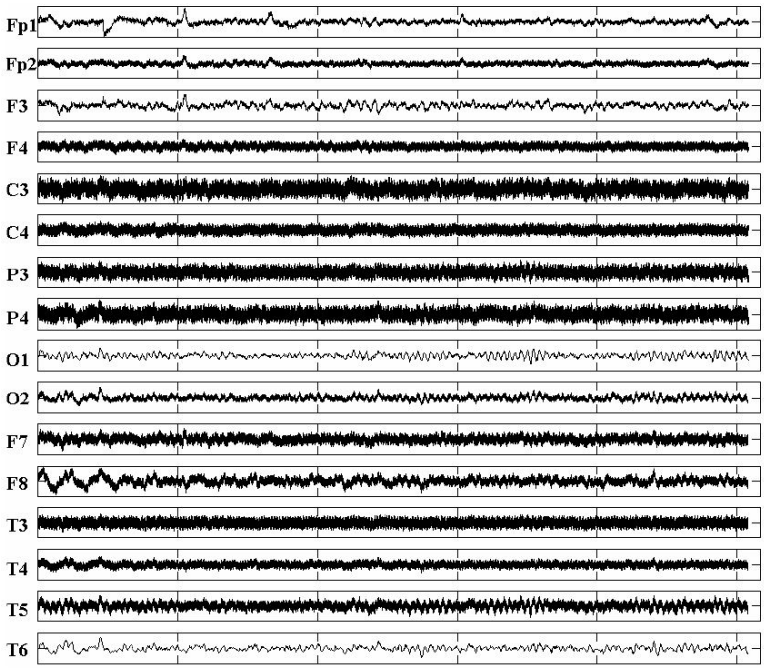

Figure 4.1: Acquired EEG signals with different artifacts

as Fp1 and Fp2 were corrupted with noise from eye blinks and most channels such as C3, C4 and F3, F4 were affected by a power line noise of 60 Hz.

4.2.1 Power Line Noise Removal

Line noise and EEG signals are generated by different sources that are independent of each other. Power spectra of the channel F4, C3, C4 P3 P4, F7, F8 and T3 are shown in figure 4.2. From this figure the presence of power line noise at 60 Hz is confirmed.

Power interference noise and the electromyographic noise encountered in EEG signal applications are usually located in the high-frequency band. Hence, high-frequency denoising by the EMD is in general carried out by partial signal reconstruction, which is premised on the fact that noise components lies in the first several IMFs. This strategy works well for those signals whose frequency content is clearly distinguished from that of noise. This basic idea is to statistically determine the index of the IMF that contains

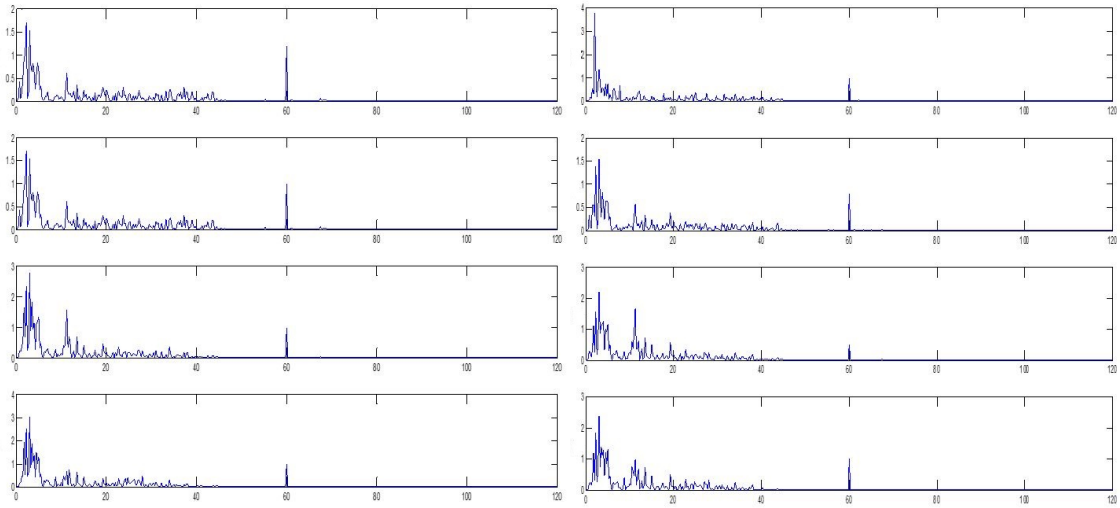

(a) (b)

Figure 4.2: Power spectrum of acquired signals (a) channels F4, C3, C4 and P3 (b) channels P4, F7, F8 and T3

most of the noise components, beginning from fine to coarse scale. Given the index, the IMFs corresponding to the noise are removed and the reconstruction of the original signal is obtained by summing up the remaining IMFs.

The channel C3 EEG signal decomposed by the EMD is shown in figure 4.3(a). Signal from C3 channel was analyzed using EMD and IMFs are shown in time domain. Here C3 electrode corresponds to the right-hand movement. The original acquired signal is shown in the top followed with IMFs from low to high order. For the left-hand movement, the channel is C4 which was also decomposed using EMD and IMFs are presented in figure 4.3(b). Though original C3 and C4 signals look similar, the differences are manifested in the component IMFs.

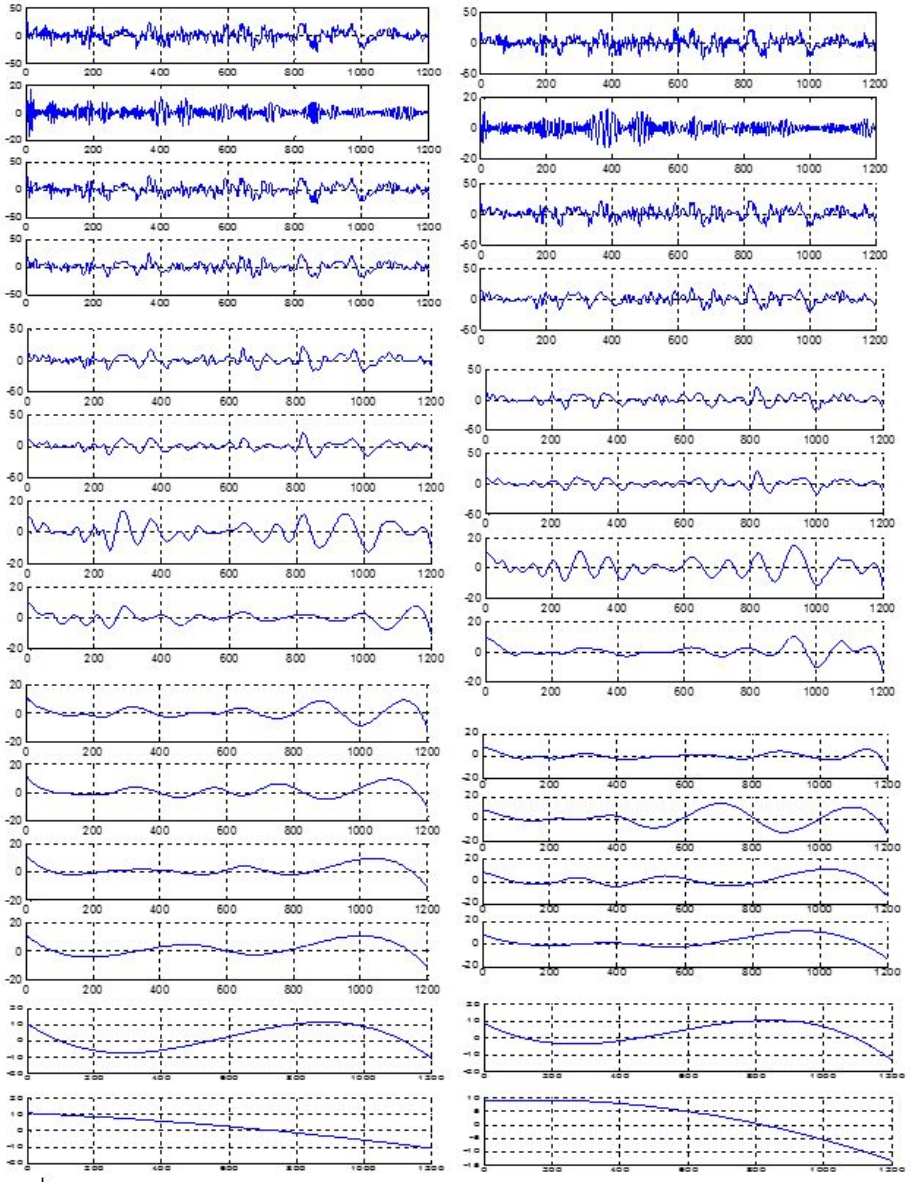

(a) (b)

Figure 4.3: EEG signals and IMFs (a) C3 signal (right hand movement) (First graph in the figure is the original signal and the last one is residue, remaining are IMFs 1 to 12(top to bottom) (b) C4 signal (left hand movement. (First graph in the figure is the original signal and the last one is residue, remaining are the IMFs 1 to 12(top to bottom))

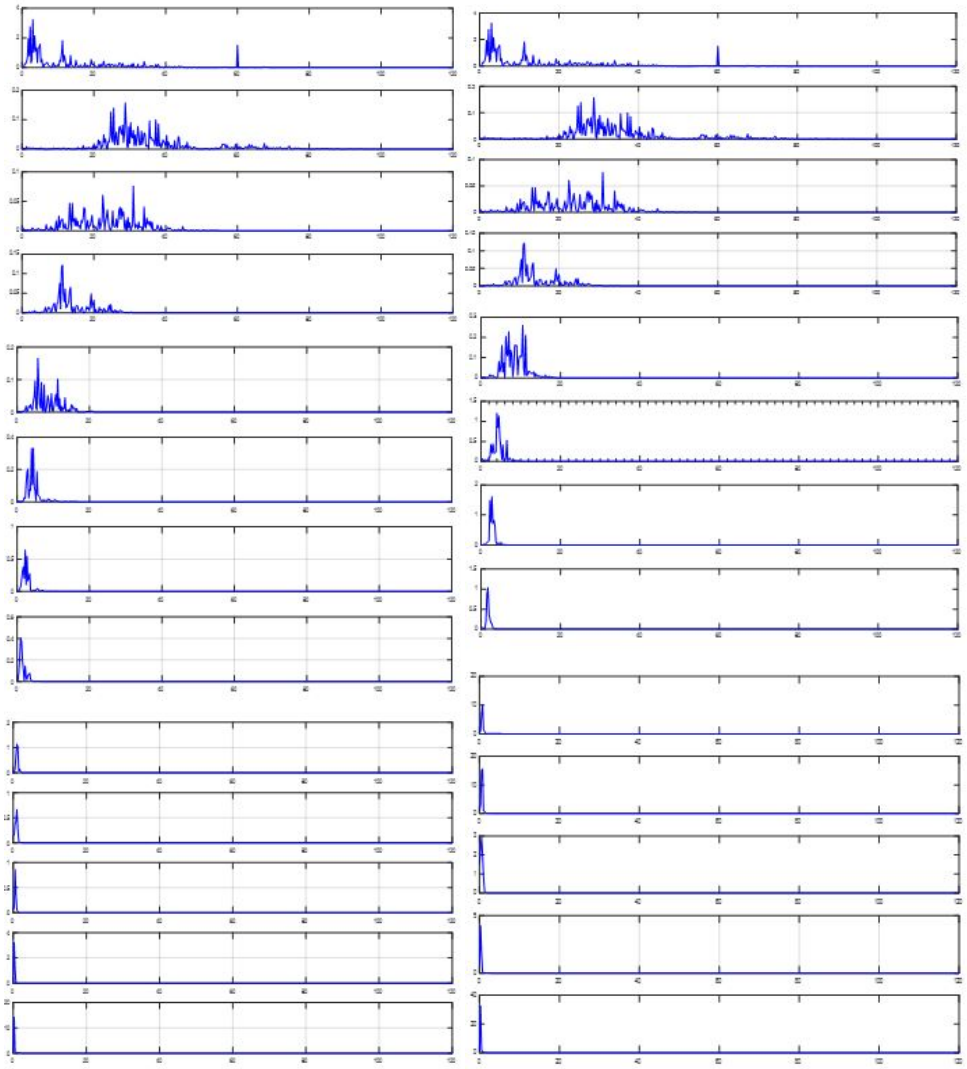

(a) Frequency (Hz) (b)

Figure 4.4: Power spectra of IMFs (a) channel C3 (b) channel C4

The power spectra of IMFs of EEG signals from channels C3 and C4 are shown in figures 4.4. The 60 Hz power line frequency, present in original signals, is eliminated in the spectra of IMFs. The differences between C3 (Right hand movement) and C4 (left-hand movement) are evident in both time domain IMFs and their corresponding frequency spectra, as shown in figures 4.3 and figures 4.4 respectively. The power spectra of the IMFs cover physiologically meaningful frequency ranges corresponding to different rhythms. For

example, the power spectra of IMFs 3-7 (rows 4-8 of figures 4.4) cover the rhythms and with some overlaps. The time domain IMFs can be processed further to extract features to distinguish different MI activities.

4.2.2 Eye Blink Artifact Removal

After the removal of power line noise from the EEG signals, the reconstructed signals are shown in figure 4.5 From this figure it is clear that the signals are still not free from artifacts.

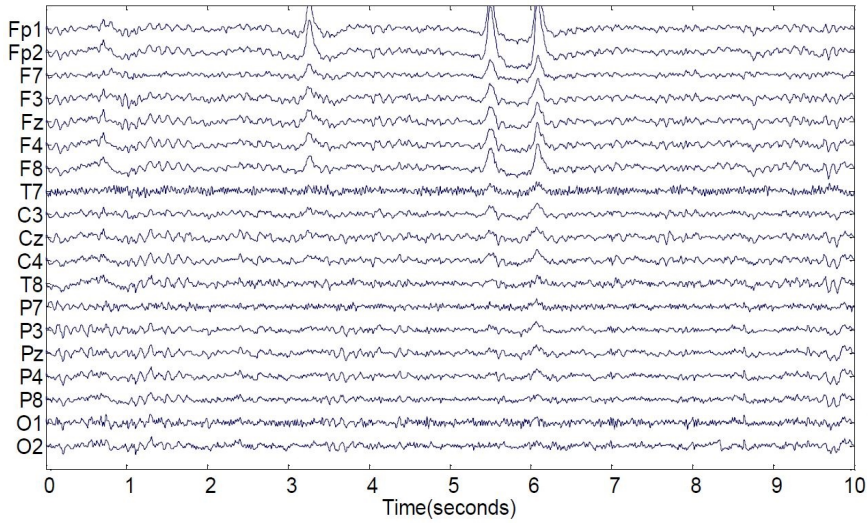

Figure 4.5: Reconstructed EEG signals after power line artifact removal

A close look at the signal from channel Fp1 in figure 4.6 reveals existence of eye blink artifacts. IMFs from EMD processed EEG signal from channel Fp1 are shown in figure 4.7.

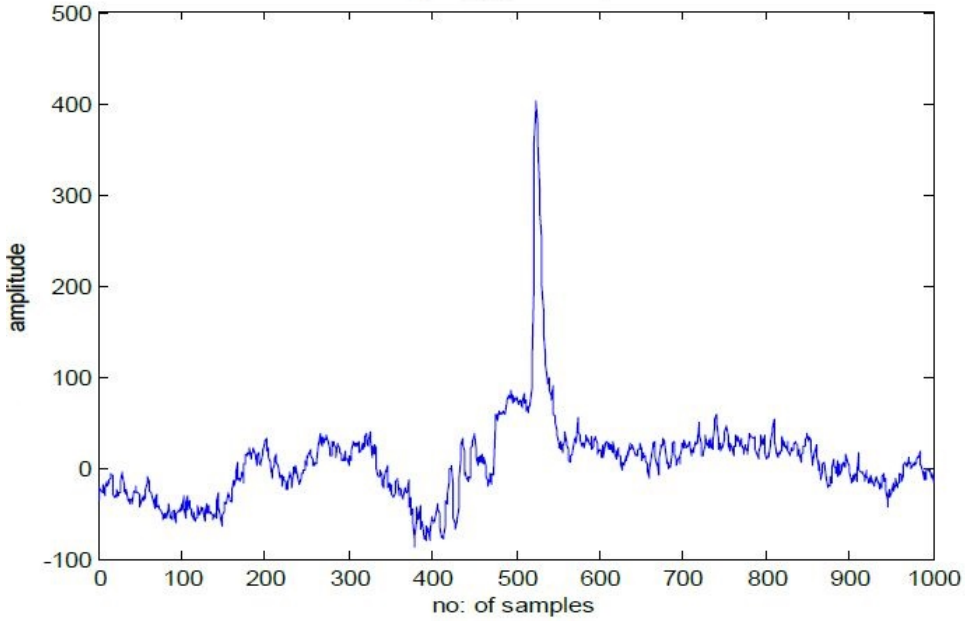

Figure 4.6: Contaminated EEG from Fp1 channel

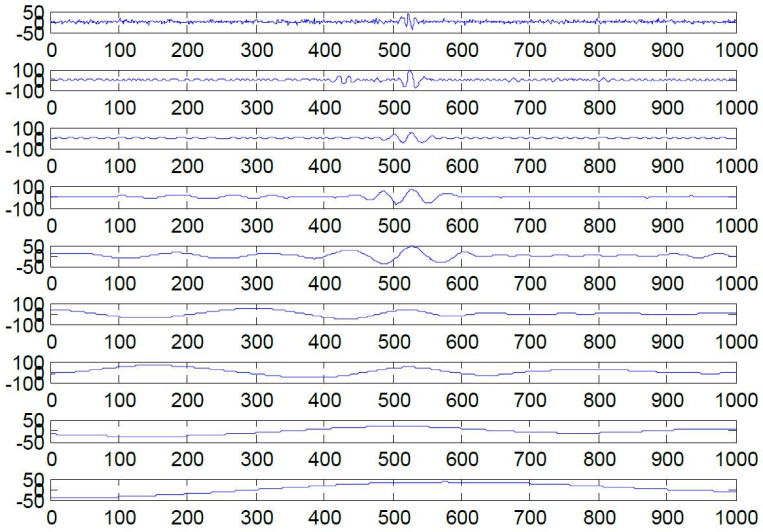

Figure 4.7: Empirical Mode Decomposition of Fp1 channel

To remove eye blink artifact sample entropy (SampEn) of IMFs were calculated for channel Fp1 and Fp2. The lower the value of SampEn for a given value of d and r, would correspond to more self-similarity in a given time series. In this work, the value of d was chosen as two. From 4.8 sudden increase in SampEn for IMF4 and IMF5 for channel Fp1 and IMF3 for channel Fp2 confirms the presence of eye blink artifacts in those IMFs.

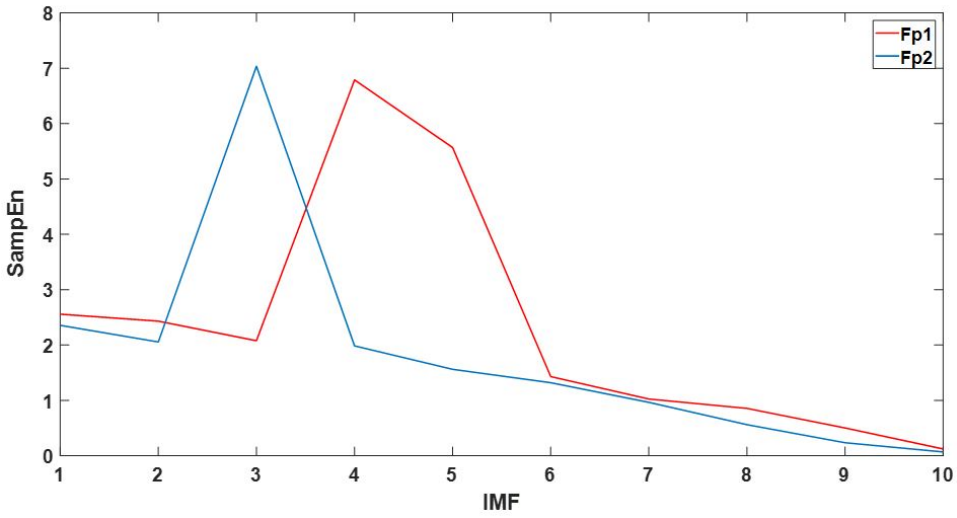

Figure 4.8: Sample entropy of channels Fp1 and Fp2

After the reconstruction of the decomposed signals, the amplitude of the artifact was reduced. After all the channels were reconstructed from the desired IMFs, deleting the IMFs corrupted with artifacts, the EEG signals were cleaner, as shown in figure 4.10 Original EEG signals were also processed in BCI2000 through ICA for removal of artifacts, and were reconstructed without the artifacts by the inverse transform of ICA. The comparison of the SNRs and the MSEs between the EMD-based method and the ICA based method after performing the artifact removal are shown in figure 4.11 and and figure 4.12, respectively. Compared to the ICA-based method, the EMD-based method gave much lower mean SNR. The MSE indicates the degree of similarity of the two signals. A smaller value of MSE indicates higher degree of similarity between two signals with less noise and artifacts.

IMFs of EEG signal from channel C3 decomposed by the EEMD and MEMD are shown

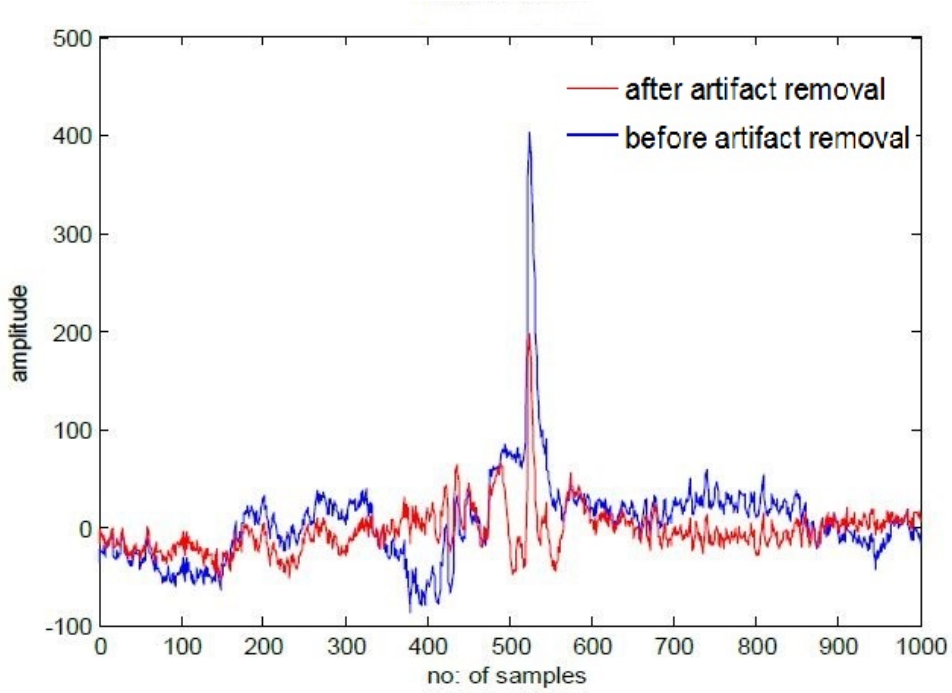

Figure 4.9: Corrected signal of Fp1 channel

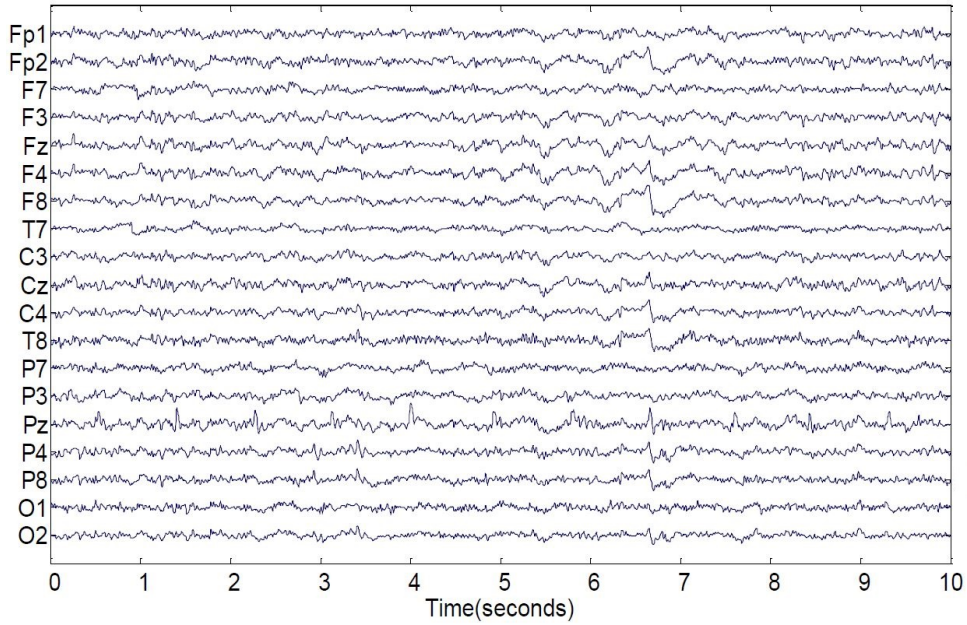

Figure 4.10: Reconstructed EEG signals after removal of artifacts

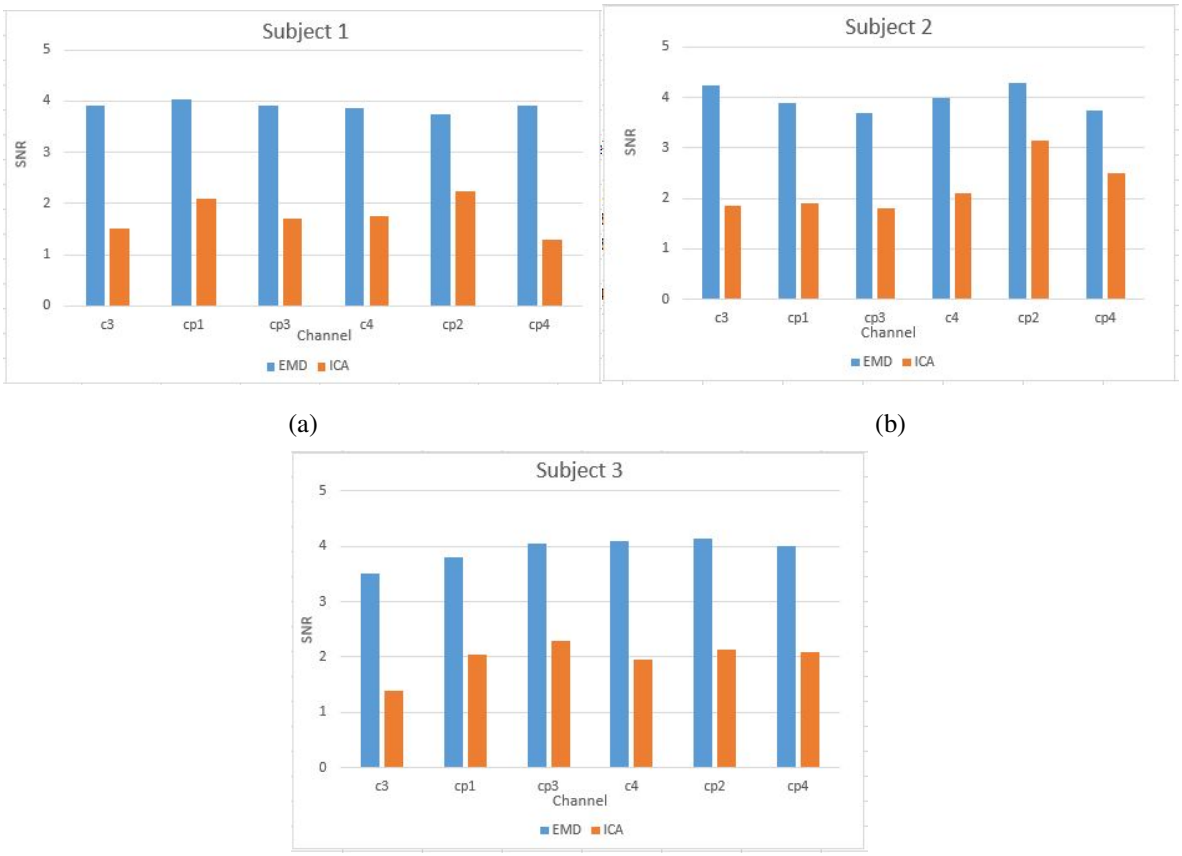

Figure 4.11: Signal to noise ratio (SNR) of EEG signals for channels C3, Cp1, Cp3, C4, Cp2, Cp4 for three subjects (a) Subject 1 (b) Subject 2 (c) Subject 3

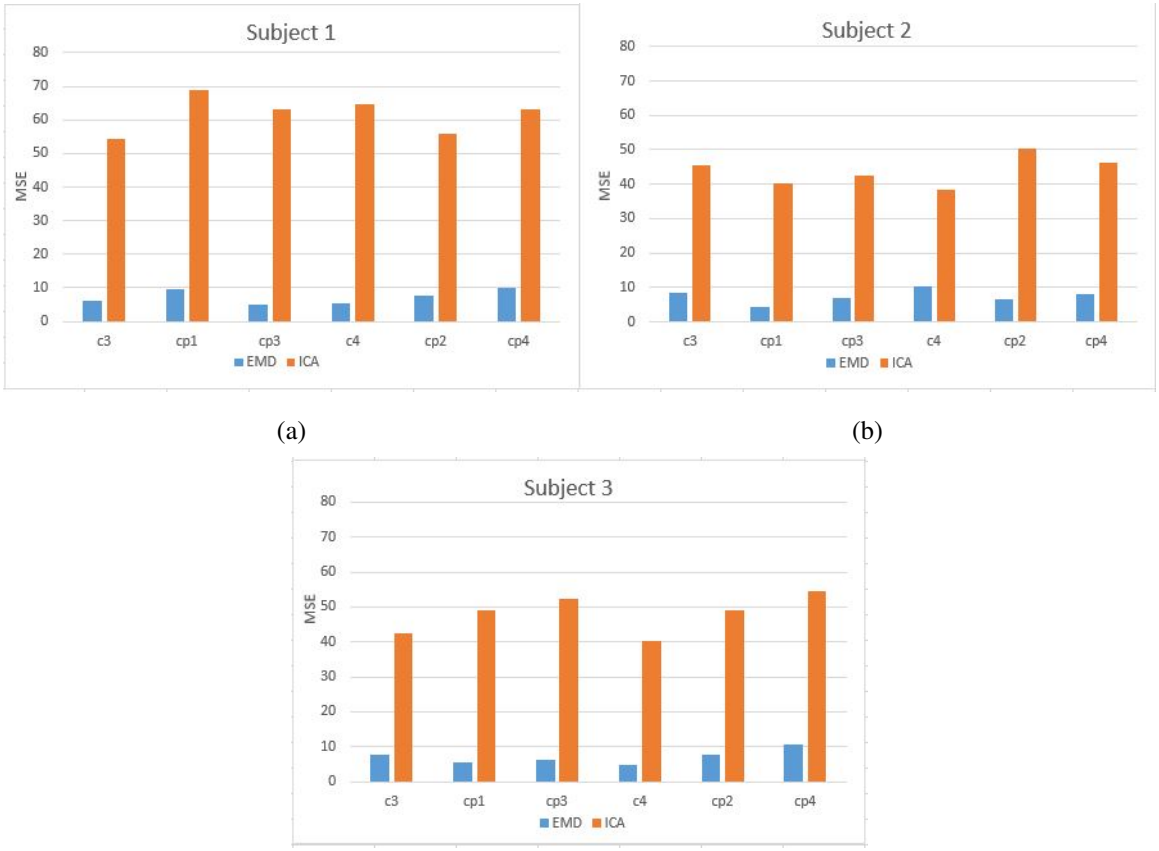

Figure 4.12: Mean Square Error (MSE) of EEG signals for channels C3, Cp1, Cp3, C4, Cp2, Cp4 for three subjects (a) Subject 1 (b) Subject 2 (c) Subject 3

in figure 4.13. EEG signal from channel C3 corresponds to the right-hand movement. The original signal is shown in the top followed with IMFs from low to high order.

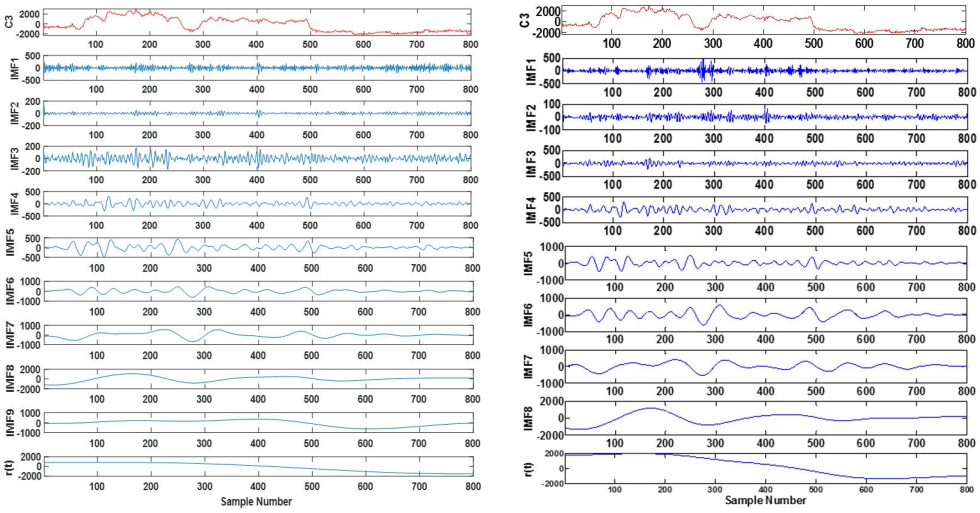

(a) (b)

Figure 4.13: IMFs of EEG signal for channel C3 (a) EEMD, and (b) MEMD

It can be noticed that applying EMD separately on EEG channels resulted in the mode-mixing and mode-misalignment in the corresponding IMFs figure 4.14, as evidenced by the overlapping of spectra of different IMFs from multiple input channels. Specifically, both IMF5 and IMF7 contributed to the mode corresponding to visual stimulus at 10 Hz. Moreover, spectra of IMF5 and IMF6 from different channels overlap, resulting in further mode-mixing. The time space was opened up different scales with the addition of white noise. With the application of MEMD to the same data set resulted in IMFs which were aligned in frequency, each containing only a single mode in time space. The addition of white Gaussian noise solves the mode mixing problem by populating the whole time-frequency space to take advantage of the dyadic filter bank behavior of the EMD. The reconstructed signal includes residual noise and different realizations of signal plus noise may produce different number of modes. To compare the effectiveness of three different

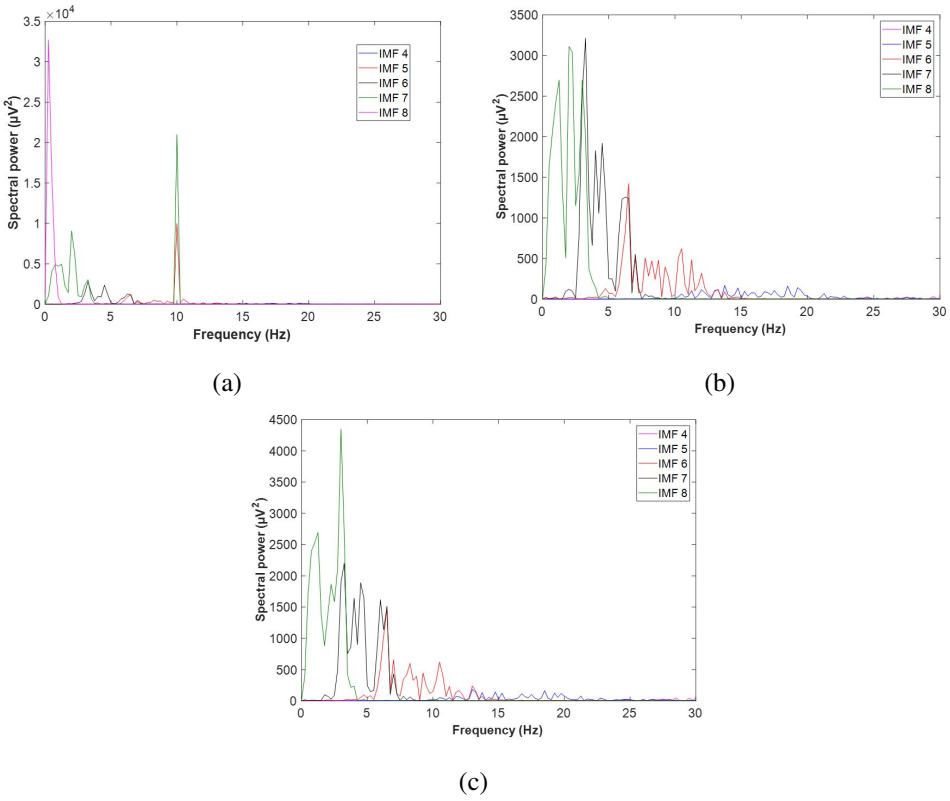

Figure 4.14: Spectral power of IMFs obtained by (a) EMD (b) EEMD and (c) MEMD

algorithms, signal to noise ratio was used.

SNRs for EMD-based methods after removing EOG and power line artifacts for subject 1 are shown in figure 4.15. Compared to the EMD algorithm, the EEMD and MEMD-based methods were more successful in removing artifacts. The higher values of SNRs for MEMD indicate less remaining noise in the pre-processed EEG signal than EMD and EEMD. It is also to be noted that MEMD had less number of IMFs than EEMD making MEMD most suitable of the three for artifact removal from the EEG signals.

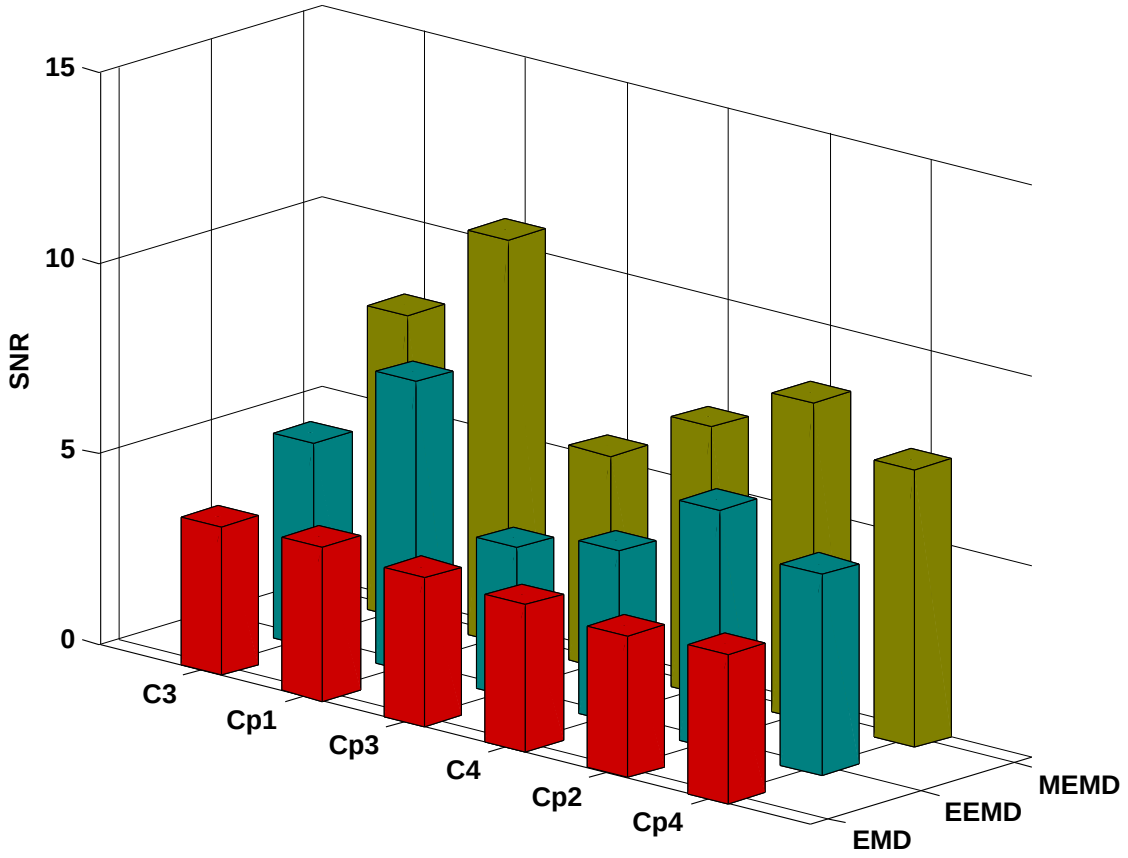

Figure 4.15: Signal to noise ratio (SNR) of EEG signals from channels C3, Cp1, Cp3, C4 Cp2, Cp4 for three algorithms : EMD, EEMD, MEMD

4.3 Feature Extraction

4.3.1 Spectral Power

To quantify EEG signal characteristics related to the different motor tasks, a well-established method of average power spectral analysis was adopted. The performance of each frequency in the power spectrum was evaluated regarding detection of different events.

4.3.1.1 Right Hand Movement

Spectral power is shown for EEG signals for several channels as a function of frequency. Comparisons of spectral power in right hand movement versus rest condition is shown in figure 4.16. Spectral power was diminished in the electrode contralateral to the actual hand movement as a result of the differential synchronization-desynchronization of the signals of the electrodes in response to the unilateral motor task. Spectral power of channels C1 and C3 decreased more compared to channels Cp1 and Cp3. So these two channels, C1 and C3 could be used for the control of right hand movement.

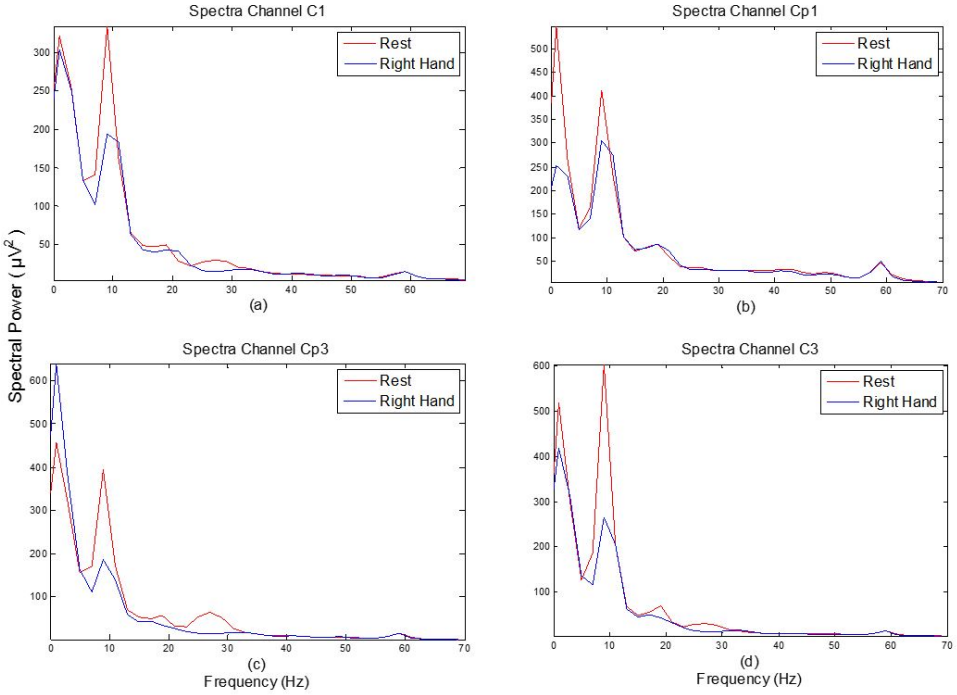

Figure 4.16: Spectral power density of EEG signals from channels (a)C1 (b)Cp1 (c)Cp3 and (d)C3

4.3.1.2 Left Hand Movement

Similarly comparisons of spectral power in left hand movement versus rest condition is shown in figure 4.17. It is seen that spectral power was diminished in the electrode

contralateral to the actual hand movement as a result of the differential synchronization-desynchronization of the electrodes in response to the unilateral motor task. Spectral power of channels C2 and C4 decreased more compared to channels Cp2 and Cp4. So these two channels, C2 and C4, could be used for the control of left hand movement.

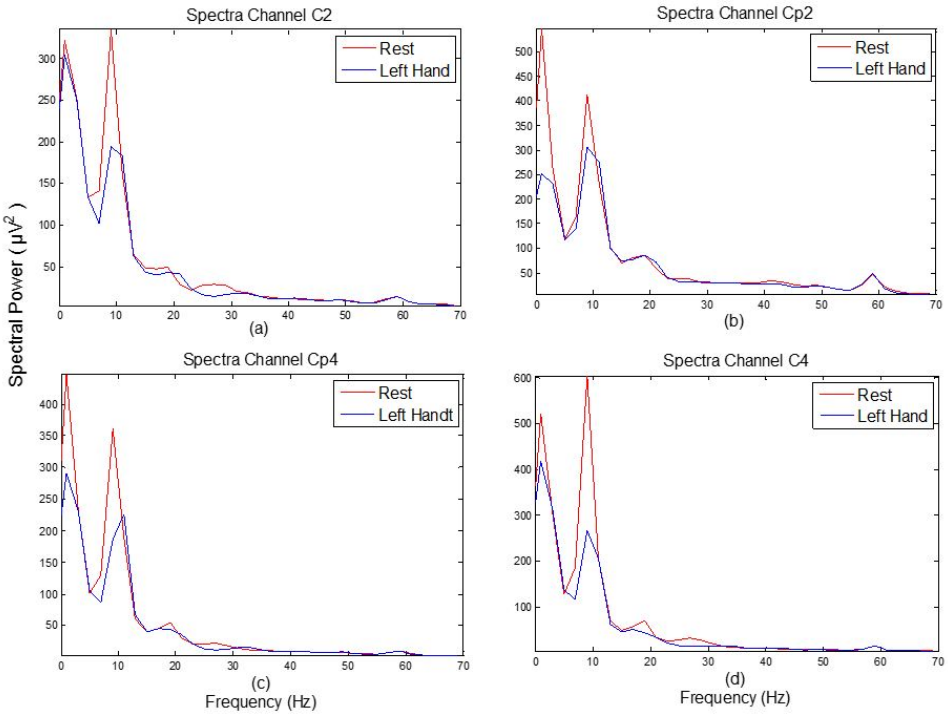

Figure 4.17: Spectral power density of EEG signals from channels (a)C2 (b)Cp2 (c)Cp4 and (d)C4

The results obtained for the R-square coefficients corresponding to imagined hands movements are presented next. Figure 4.18 shows the head topo-frequency range from 8 to 24 Hz of most active R-square coefficients corresponding to imagined movement of right hand for subject 1 with the color bar representing the value of R-square coefficient. Among these frequency bands, the most prominent C3 channel (compared to other channels) was at a frequency of 16 Hz. So at 16 Hz, brain area around channel C3 was most active compared to area around it for right hand movement for subject 1.

Figure 4.19 shows the head topo-frequency range from 8 to 24 Hz of most active

R-square coefficient corresponding to imagined movement of left hand for subject 1, with color bar showing the value of R-square coefficient. Among these frequency bands, the most prominent C3 channel (compared to other channels) was at a frequency of 14 Hz. So at 14 Hz, brain area around channel C4 is most active compared to area around it for left hand movement for subject 1.

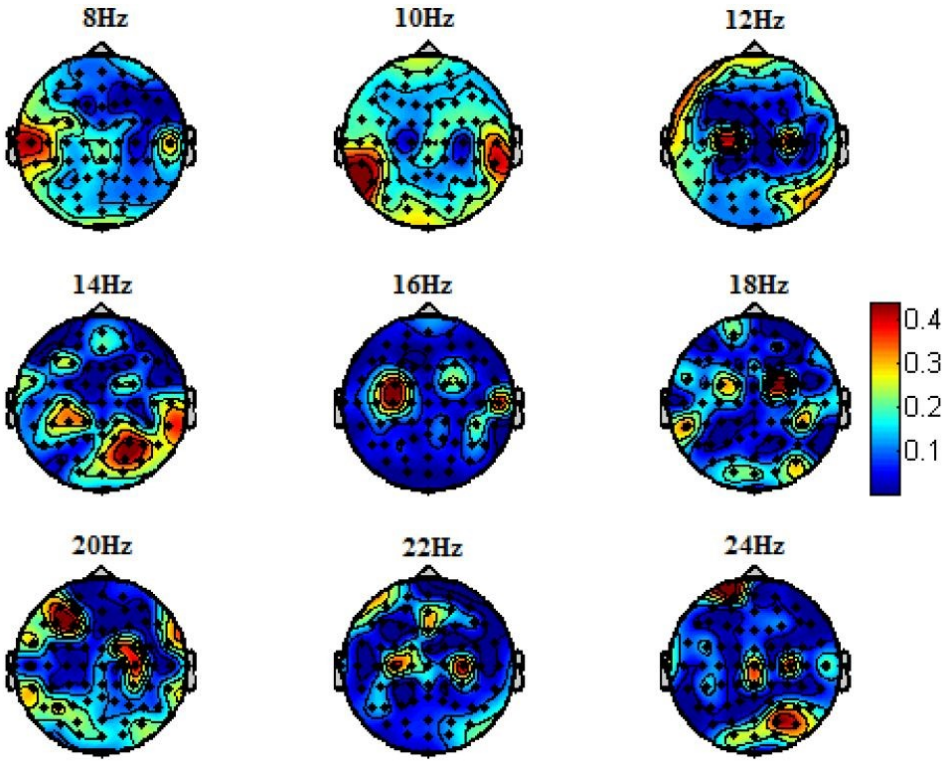

Figure 4.18: R square of Right hand movement at different frequencies

Figure 4.18 and 4.19 show even concrete evidence observed in neurophysiology study that the optimal frequency change with activity, especially in the imagination tasks (MI).

The active frequency band is expected to change from subject to subject and even from a class to another class of imagination movement. A MI-BCI based on fixed channel location may result in lower accuracy because of EEG signal is distributed over an area rather than a fixed position. While multi-channel BCI system could also be affected by the artifacts from multiple channels.

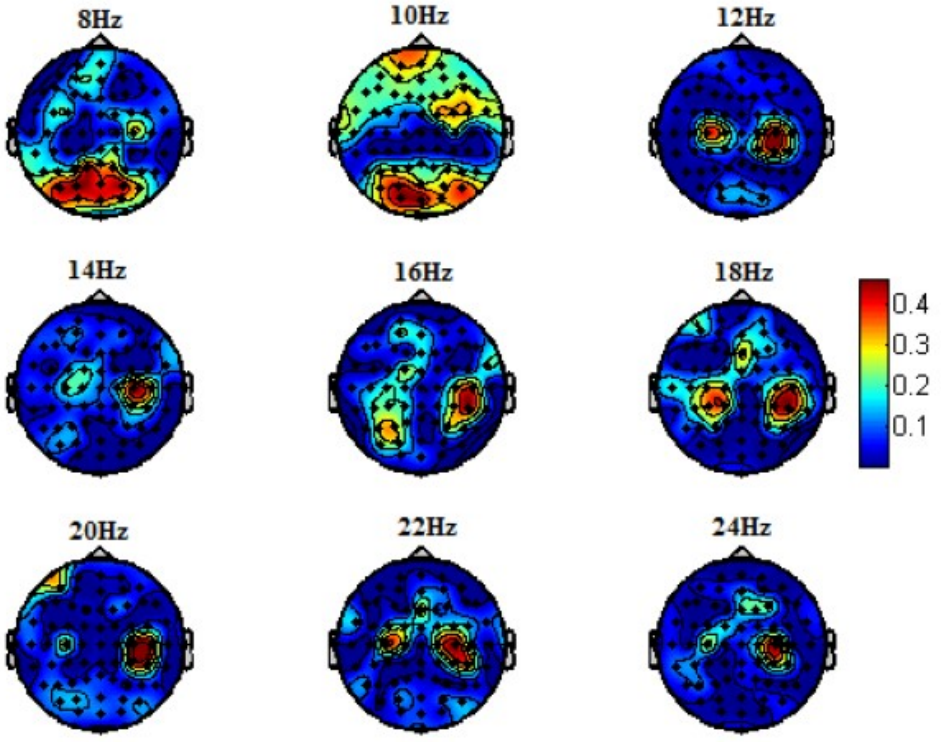

Figure 4.19: R square of Left hand movement at different frequencies

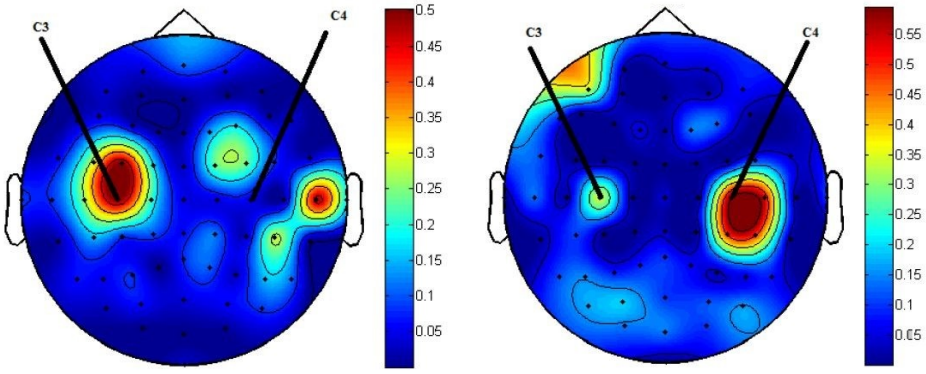

(a) (b)

Figure 4.20: R square topography corresponds to (a)right hand movement at 16 Hz (b)left hand movement at 14 Hz

4.3.1.3 Both Hands Movement

Change in oscillation in channel C3 and C4 can be observed in figure 4.21. R square topography of both hands movement at the same time is shown in figure 4.22. R square topography describes the stimulation of EEG electrode for the movement of both hands. EEG signals from C3 and C4 electrodes had the highest R square values. Spectral power of channel C3 and C4 decreased at a frequency of 14 Hz.

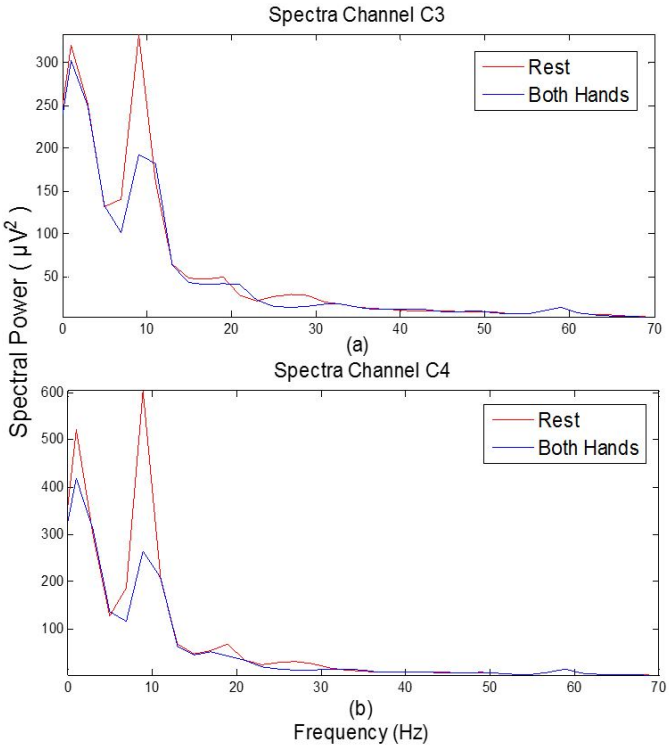

Figure 4.21: Spectral power density EEG signals for both hands movement (a)channel C3 and (b)channel C4

4.3.1.4 Both Feet Movement

R square topography for the both feet movement is shown in figure 4.24 which describes the stimulation of EEG electrode for the movement of feet are in central region of the brain. Cz and Cpz electrodes had the highest R square values. Spectral power of EEG signals for

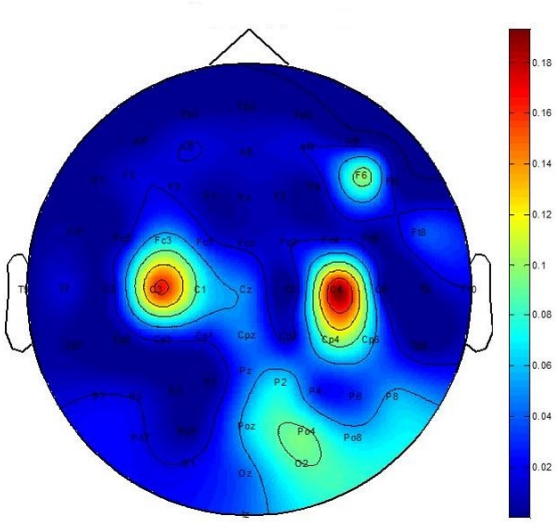

Figure 4.22: R square of Both hands movement at 14 Hz

channels Cz and Cpz decreased at a frequency of 10 Hz. Change in oscillation in channel C3 and C4 can be observed in figure 4.23

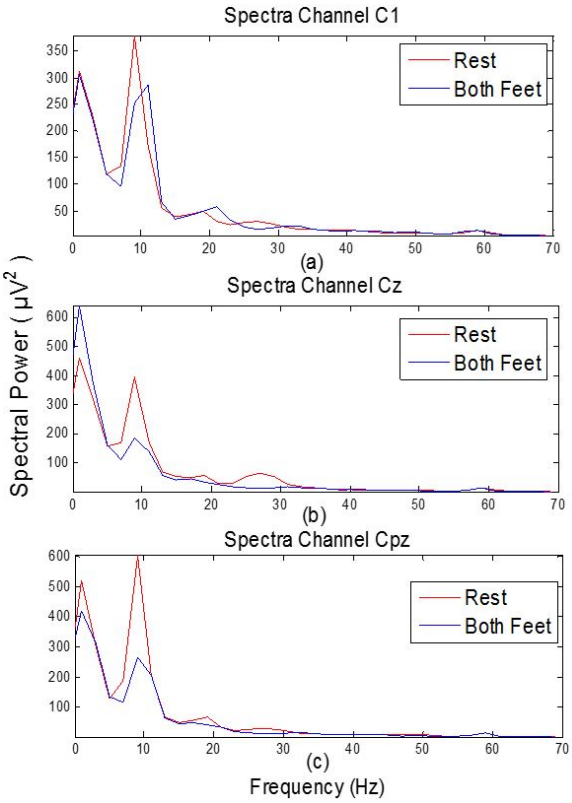

Figure 4.23: Spectral power density of channel for both feet movement(a)C1 (b) Cz and (b)Cpz

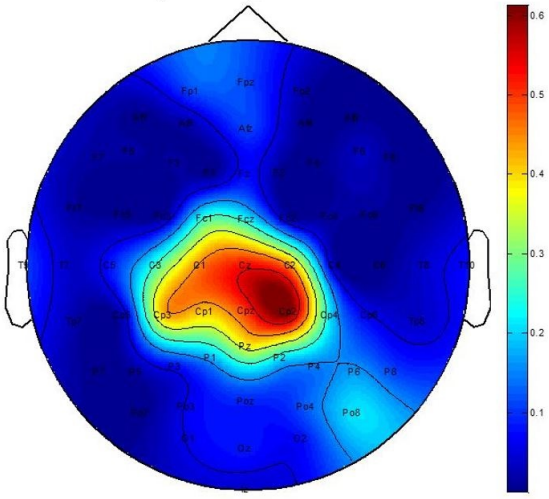

Figure 4.24: R square of Both feet movement at 10 Hz

4.3.1.5 Comparison Between Actual Movement and Imagined Movement

A comparison between the spectral power of actual movement and imagined movement for both hands is shown in figure 4.25 and 4.26. At a frequency of 10 Hz, C1 and C3 showed the closest spectral power for right hand movement. Channels having the lowest difference of spectral power between the actual movement and the imagined movement is shown in these figures, similarly C2 and C4 for left hand and C3 and C4 together for the both hands movement.

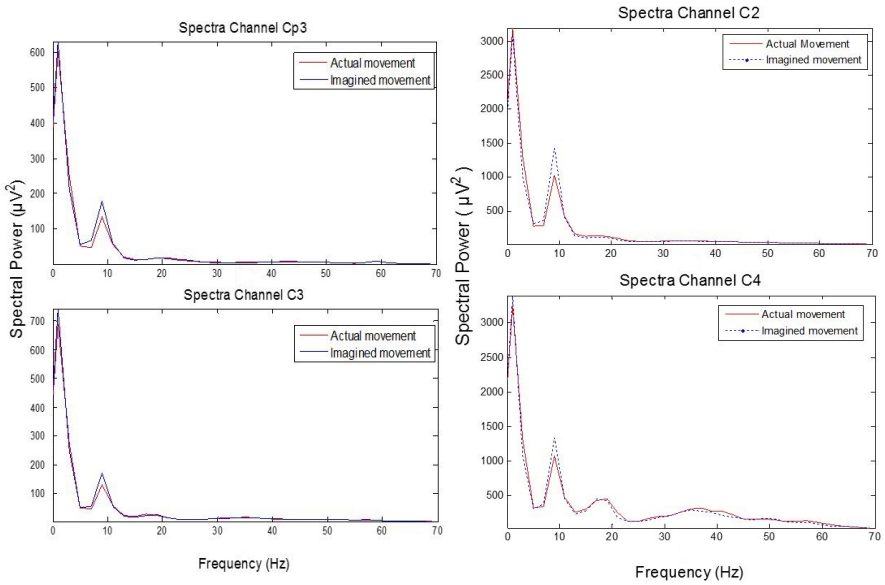

(a) (b)

Figure 4.25: Spectral power density for imagined(a)right hand movement (b) left hand movement

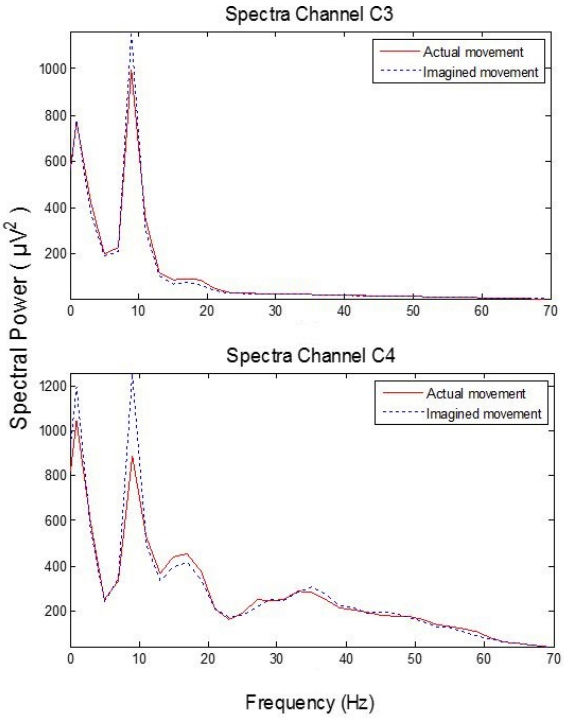

Figure 4.26: Spectral power density for imagined both hands movement

4.3.2 EMD Based Feature Selection

A direct nonlinear approach was adopted to extract the more relevant IMFs corresponding to the different frequency components in the mu and beta bands and to obtain the band power for using these as features for mental task classification. EMD method was applied to the EEG data defined previously. The EEG data for each subject were composed of 100 trials corresponding to left hand movement imaginations (C4) and 100 trials corresponding to right hand movement (C3).

4.3.2.1 Band Power

Figure 4.27 shows the result of EMD decomposition for subject 1. Each channel is decomposed into different IMFs and one residue.

To analyze the different characteristics of each IMF, power spectrum density (PSD)

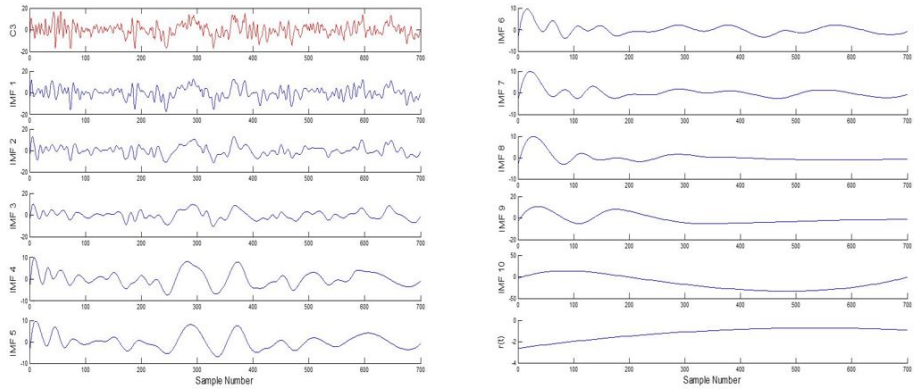

(a)

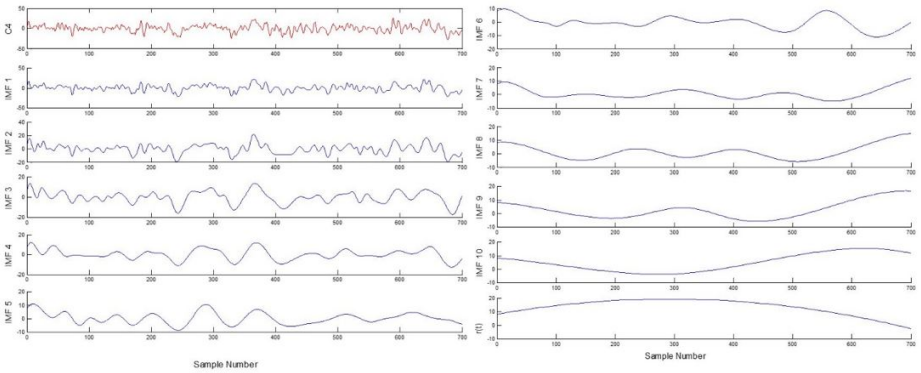

(b)

Figure 4.27: Intrinsic mode functions of (a) channel C3 (b) channel C4

method was applied. This method was applied to each IMF to calculate and find the active frequency bands such as the mu and beta rhythms. Figure 4.28 and 4.29 show the PSD in each IMF in the two channels C3 and C4. The characteristics of the active frequency bands corresponding to mu and beta are located only in IMF1, IMF2 of C3 and C4. Concerning subject 1, the active frequency bands were located only in IMF1, IMF2 and IMF3 of C3 and C4. Therefore, the new signal was reconstructed by keeping only the two first IMFs for subject 2 and only three first IMFs for subject 1. When the band power of actual movement and imagined movement matched for these IMFs, the imagined movement was considered as successful. In the data acquisition stage every motor imagery task was done 20 times in one session and there was 5 different sessions giving 100 data sets. The accuracy was found by comparing how many imagined movement could be identified during the imagined movement task session.

A feature extraction method based on the Empirical Mode Decomposition (EMD) and the band power (BP) was proposed to keep only the active frequency band powers corresponding to mu and beta rhythms in BCI-related mental task EEG signals. The feature extraction process was done in three-stages: in the first stage EMD was applied on the raw EEG signals to obtain the Intrinsic Mode Functions (IMF). The second stage reconstructed the relevant signal by keeping only the IMFs which contained the active frequency bands. The third stage calculated the BP of the active frequencies in the relevant signal.

4.3.2.2 Sample Entropy

Sample Entropy of different intrinsic mode function was calculated for the selected channel more correlation with the movement task. Table 4.1 describes the sample entropy of the IMFs for subject 1. When the sample entropy for imagined movement matched with the actual movement then it was considered as successful identification.

From figure 4.30 and 4.31 it can be seen that accuracy for the mental task recognition

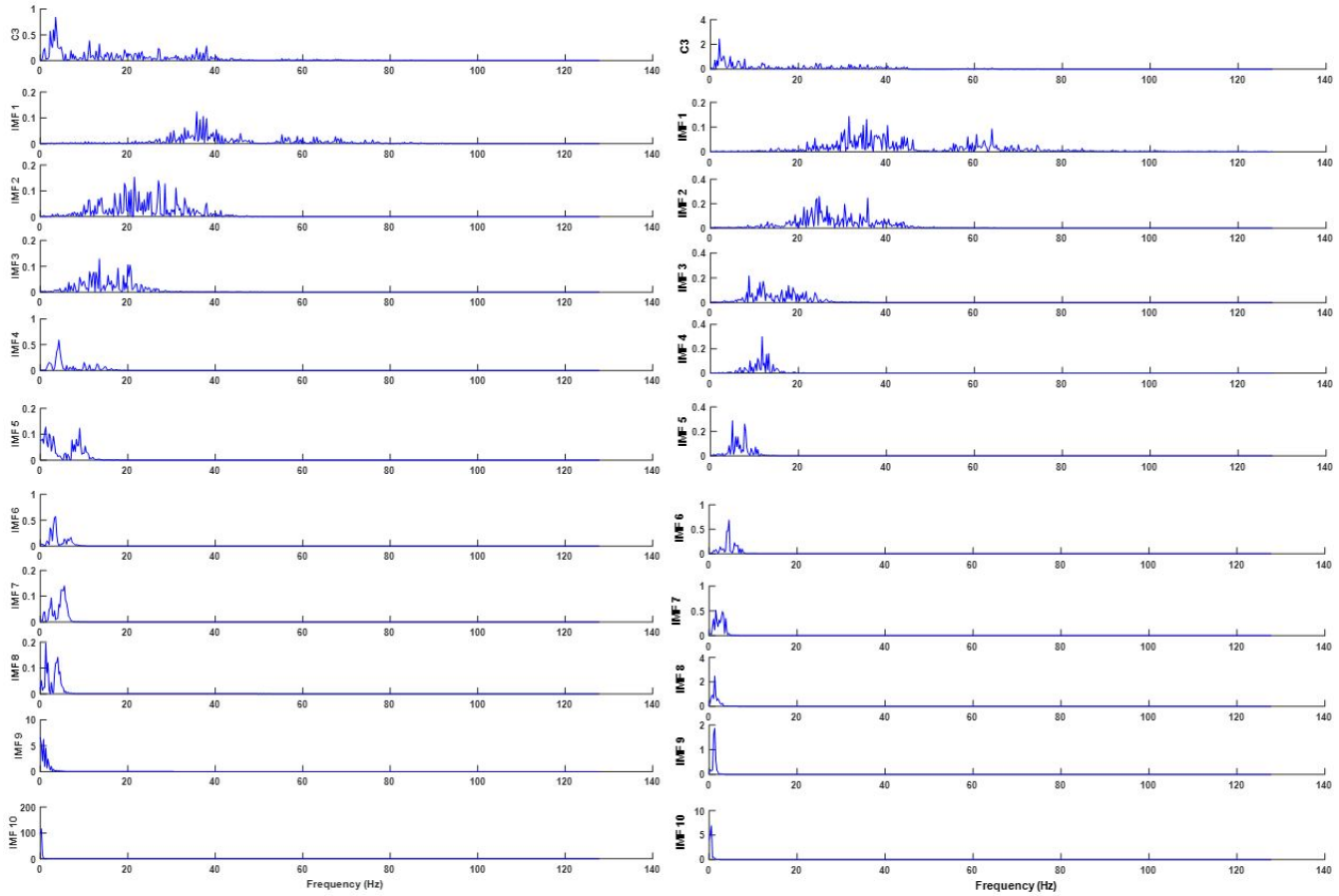

(a) (b)

Figure 4.28: PSD (dB/Hz) vs. frequency (Hz) of each IMF for channel C3 (a) actual movement and (b) imagined movement

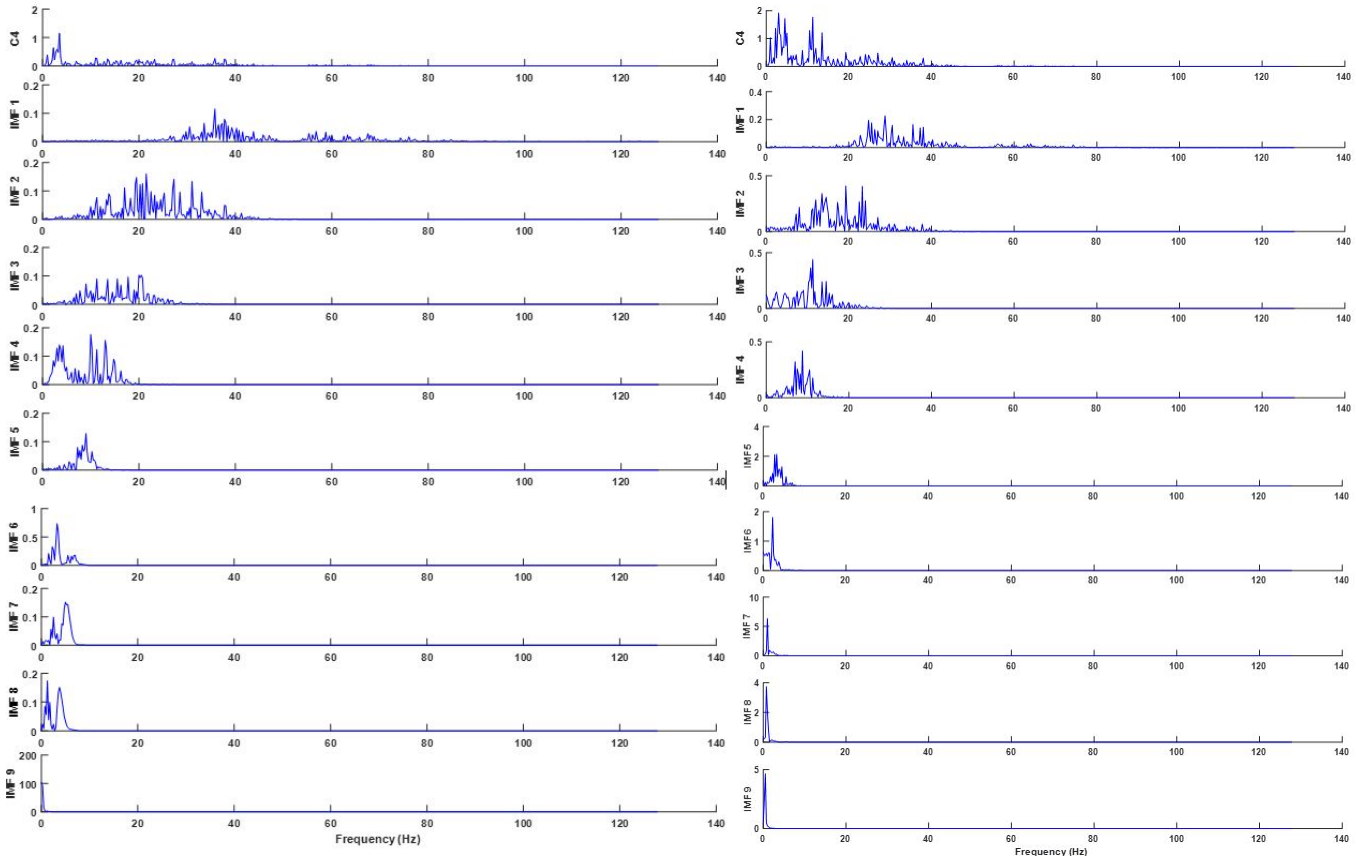

(a) (b)

Figure 4.29: PSD (dB/Hz) vs. frequency (Hz) of each IMF for channel C4 (a) actual movement and (b) imagined movement

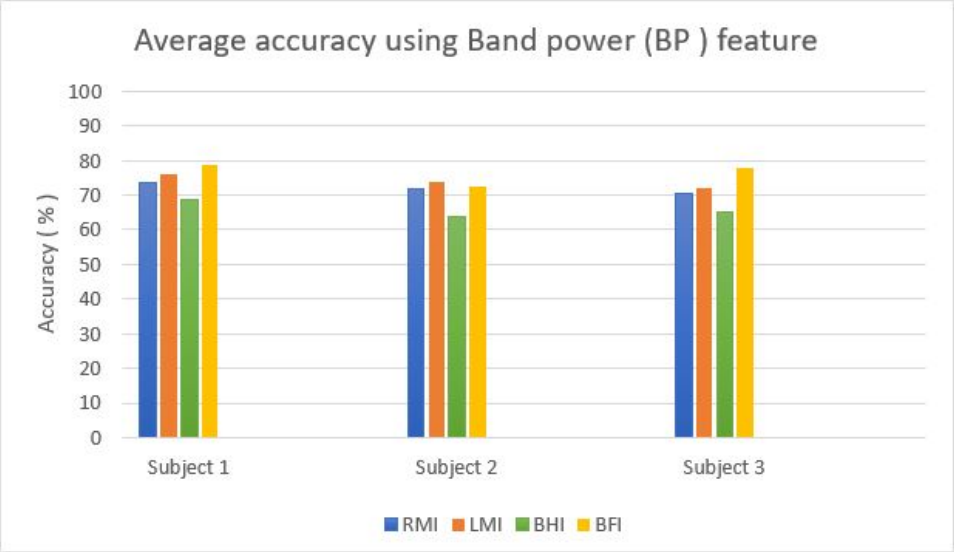

Figure 4.30: Average accuracy using Band power (BP) as feature for four tasks

Table 4.1: Sample Entropy of Intrinsic mode functions for actual and imagined movements

IMF	C3 (Right hand)		Cp3(Right hand)		C4(Left hand)		Cp4(Left hand)		Cz(Feet)	
	Actual	Imagined	Actual	Imagined	Actual	Imagined	Actual	Imagined	Actual	Imagined
IMF1	2.6911	2.632	2.936	2.887	3.975	4.15	3.569	3.447	5.585	5.664
IMF2	2.593	2.601	2.8235	2.808	3.523	3.389	3.032	3.088	5.032	5.078
IMF3	2.3958	2.256	2.568	2.58	3.056	3.075	2.865	2.912	4.56	4.887
IMF4	2.211	2.301	2.321	2.35	2.804	2.789	2.407	2.508	4.026	4.157
IMF5	1.845	1.814	2.012	2.08	2.457	2.501	1.79	1.763	3.51	3.42
IMF6	1.277	1.298	1.532	1.602	2.039	2.042	1.045	1.086	3.182	3.187
IMF7	0.6229	.823	1.023	1.08	1.85	1.887	.7403	.822	2.15	2.309
IMF8	0.1837	.18	.503	.606	1.26	1.204	.236	.295	1.68	1.702
IMF9	0.0497	.05	.178	.205	.95	.884	.084	.094	1.064	1.118
IMF10	0.0108	.009	.0806	.0911	.1256	.133	.022	.0335	.508	.576

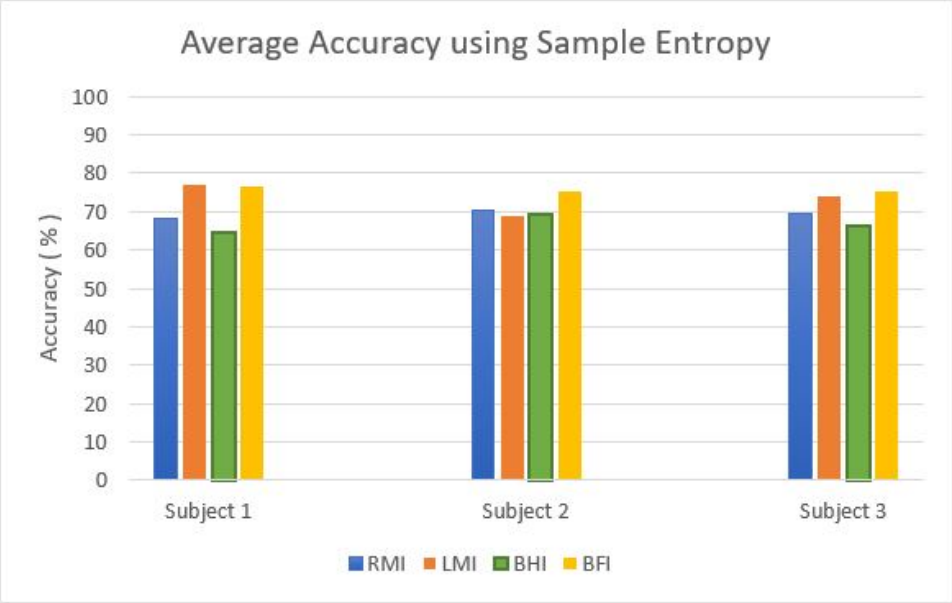

Figure 4.31: Average accuracy using Sample Entropy (SampEn) as feature for four tasks

was higher for the band power feature than sample entropy. Both feet recognition rate had a significantly higher accuracy rates compared to the other motor imagery based task as the signal was from the vertex zone (Cz and Cpz electrodes).

Accuracy of mental task identification is shown in figure 4.32. Though EMD algorithm was found to be more effective in noise reduction figure 4.11 and 4.12, but for the feature extraction EMD had lower accuracy than CSP method. The most possible reason for that may be the mode mixing criteria of empirically decomposed signal. The reasons of mode mixing mainly include high frequency weak signal in noise or discontinuous signal interference, resulting in the extreme value point of the signal distribution confusion and mixed signal's amplitude and frequency relationship.

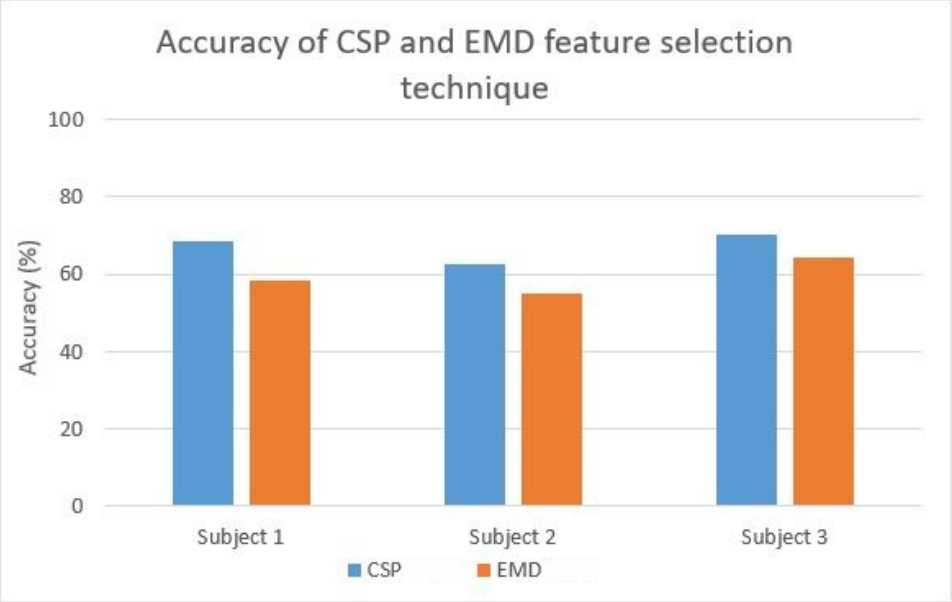

Figure 4.32: Comparison of CSP and EMD feature extraction technique

CHAPTER 5

CONCLUSION

5.1 Summary of Present Work

In this study a signal processing technique, namely empirical modal decomposition (EMD), and two its variants, ensemble EMD (EEMD) and multivariate EMD (MEMD), were proposed for artifact removal and feature extraction from EEG signals in motor imagery (MI) based BCI applications. With application of these signal processing techniques to pre-process EEG signals, signal to noise ratio (SNR) improved significantly over the independent component analysis (ICA) used in BCI2000. In summary, the following objectives were fulfilled:

- Artifacts were removed from the raw EEG signals acquired for different actual motor actions and MI activities by using empirical mode decomposition (EMD).
- Extensions of EMD algorithm such as EEMD and MEMD were used to overcome the mode mixing and mode misalignment problem associated with EMD algorithm.
- A comparative analysis was carried out to remove artifacts from raw EEG signal based on EMD and its variants, EEMD and MEMD with the CSP based approach.
- Extraction of features (r square coefficient, spectral power, band power and sample entropy) was performed from the pre-processed EEG signals for motor task identification.
- Actual motor actions and MI activities were identified and classified using extracted features.
- A comparison was made between the accuracy of mental task identification for EMD and CSP based approaches.

After observing all the findings from above analysis it can be concluded that the hypothesis "if suitable algorithms are used for artifact removal and feature extraction from motor imagery based EEG signals, the signal to noise ratio (SNR) of pre-processed EEG signals will improve leading to distinct features for better identification and classification of MI-BCI activities" was successfully tested. Further work is planned for next stage to use the artifact-free EEG signals for characterization and identification of motor imagery (MI) in the context of MI based brain-computer interface (BCI) applications.

5.2 Scope For Future Work

This work laid the foundation of MI-BCI research in B-IRIS lab by integrating acquisition of EEG signals with pre- and post-processing of signals for actual and imagined motor actions. There are tasks related to this research that need to be improved and can be further applied to get better identification of motor imagery (MI) tasks. Some on-going and future directions of extending the research are outlined as follows:

- More features, in addition to band power (BP) and sample entropy (SampEn), can be extracted from artifact-free pre-processed (through EMD, EEMD and MEMD) EEG signals.

- Extended group of extracted features can be used in support vector machine (SVM) to identify and classify MI activities. The performance of EMD, EEMD and MEMD can be compared on the basis of classification success through the corresponding extracted features.

- Features extracted from EMD, EEMD, MEMD approach could be used in combination with that obtained from CSP based approach from BCI2000 for identification and classification of MI activities using support vector machine.

- Other classifiers can be considered to compare the classification performance with SVM.
- The classification stage can be extended to next phase, namely, actuation and control of external devices through motor imagery based BCI.
- The MI-BCI research can be integrated with the cloud computing framework of B-IRIS lab.

REFERENCES

[1] M. A. Lebedev and M. A. Nicolelis, "Brain–machine interfaces: past, present and future," *TRENDS in Neurosciences*, vol. 29, no. 9, pp. 536–546, 2006.

[2] J. N. Knight, "Signal fraction analysis and artifact removal in eeg," Ph.D. dissertation, Colorado State University, 2003.

[3] F. Lotte, M. Congedo, A. Lécuyer, F. Lamarche, and B. Arnaldi, "A review of classification algorithms for eeg-based brain–computer interfaces," *Journal of neural engineering*, vol. 4, no. 2, p. R1, 2007.

[4] A. Roman-Gonzalez, "Eeg signal processing for bci applications," in *Human–Computer Systems Interaction: Backgrounds and Applications 2*. Springer, 2012, pp. 571–591.

[5] T. Bonaci, J. Herron, C. Matlack, and H. J. Chizeck, "Securing the exocortex: A twenty-first century cybernetics challenge," in *Norbert Wiener in the 21st Century (21CW), 2014 IEEE Conference on*. IEEE, 2014, pp. 1–8.

[6] F. Lotte, L. Bougrain, and M. Clerc, "Electroencephalography (eeg)-based brain–computer interfaces," *Wiley Encyclopedia of Electrical and Electronics Engineering*, 2015.

[7] C. Park, D. Looney, N. ur Rehman, A. Ahrabian, and D. P. Mandic, "Classification of motor imagery bci using multivariate empirical mode decomposition," *IEEE Transactions on neural systems and rehabilitation engineering*, vol. 21, no. 1, pp. 10–22, 2013.

[8] M. Wairagkar, "Motor imagery based brain computer interface (bci) using artificial neural network classifiers," in *Proceedings of the British Conference of Undergraduate Research*, vol. 1, 2014.

[9] N. E. Huang, Z. Shen, S. R. Long, M. C. Wu, H. H. Shih, Q. Zheng, N.-C. Yen, C. C. Tung, and H. H. Liu, "The empirical mode decomposition and the hilbert spectrum for nonlinear and non-stationary time series analysis," in *Proceedings of the Royal Society of London A: Mathematical, Physical and Engineering Sciences*, vol. 454, no. 1971. The Royal Society, 1998, pp. 903–995.

[10] Z. Wu and N. E. Huang, "Ensemble empirical mode decomposition: a noise-assisted data analysis method," *Advances in adaptive data analysis*, vol. 1, no. 01, pp. 1–41, 2009.

[11] N. Ur Rehman and D. P. Mandic, "Filter bank property of multivariate empirical mode decomposition," *IEEE Transactions on Signal Processing*, vol. 59, no. 5, pp. 2421–2426, 2011.

[12] Y. Wang, S. Gao, and X. Gao, "Common spatial pattern method for channel selelction in motor imagery based brain-computer interface," in *Engineering in Medicine and Biology Society, 2005. IEEE-EMBS 2005. 27th Annual International Conference of the*. IEEE, 2006, pp. 5392–5395.

[13] A. P. Georgopoulos, J. F. Kalaska, R. Caminiti, and J. T. Massey, "On the relations between the direction of two-dimensional arm movements and cell discharge in primate motor cortex," *Journal of Neuroscience*, vol. 2, no. 11, pp. 1527–1537, 1982.

[14] D. M. Taylor, S. I. H. Tillery, and A. B. Schwartz, "Direct cortical control of 3d neuroprosthetic devices," *Science*, vol. 296, no. 5574, pp. 1829–1832, 2002.

[15] L. F. Nicolas-Alonso, R. Corralejo, J. Gomez-Pilar, D. Álvarez, and R. Hornero, "Adaptive stacked generalization for multiclass motor imagery-based brain computer interfaces," *IEEE Transactions on Neural Systems and Rehabilitation Engineering*, vol. 23, no. 4, pp. 702–712, 2015.

[16] S. Musallam, B. Corneil, B. Greger, H. Scherberger, and R. Andersen, "Cognitive control signals for neural prosthetics," *Science*, vol. 305, no. 5681, pp. 258–262, 2004.

[17] F. Cincotti, D. Mattia, F. Aloise, S. Bufalari, G. Schalk, G. Oriolo, A. Cherubini, M. G. Marciani, and F. Babiloni, "Non-invasive brain–computer interface system: towards its application as assistive technology," *Brain research bulletin*, vol. 75, no. 6, pp. 796–803, 2008.

[18] J. R. Wolpaw, G. E. Loeb, B. Z. Allison, E. Donchin, O. F. do Nascimento, W. J. Heetderks, F. Nijboer, W. G. Shain, and J. N. Turner, "Bci meeting 2005-workshop on signals and recording methods," *IEEE Transactions on neural systems and rehabilitation engineering*, vol. 14, no. 2, pp. 138–141, 2006.

[19] J. Mellinger, G. Schalk, C. Braun, H. Preissl, W. Rosenstiel, N. Birbaumer, and A. Kübler, "An meg-based brain–computer interface (bci)," *Neuroimage*, vol. 36, no. 3, pp. 581–593, 2007.

[20] M. Besserve, K. Jerbi, F. Laurent, S. Baillet, J. Martinerie, and L. Garnero, "Classification methods for ongoing eeg and meg signals," *Biological research*, vol. 40, no. 4, pp. 415–437, 2007.

[21] N. Weiskopf, K. Mathiak, S. W. Bock, F. Scharnowski, R. Veit, W. Grodd, R. Goebel, and N. Birbaumer, "Principles of a brain-computer interface (bci) based on real-time functional magnetic resonance imaging (fmri)," *IEEE transactions on biomedical engineering*, vol. 51, no. 6, pp. 966–970, 2004.

[22] S. M. Coyle, T. E. Ward, and C. M. Markham, "Brain–computer interface using a simplified functional near-infrared spectroscopy system," *Journal of neural engineering*, vol. 4, no. 3, p. 219, 2007.

[23] E. C. Leuthardt, K. J. Miller, G. Schalk, R. P. Rao, and J. G. Ojemann, "Electrocorticography-based brain computer interface-the seattle experience," *IEEE Transactions on Neural Systems and Rehabilitation Engineering*, vol. 14, no. 2, pp. 194–198, 2006.

[24] P. Herman, G. Prasad, T. M. McGinnity, and D. Coyle, "Comparative analysis of spectral approaches to feature extraction for eeg-based motor imagery classification," *IEEE Transactions on Neural Systems and Rehabilitation Engineering*, vol. 16, no. 4, pp. 317–326, 2008.

[25] L. R. Hochberg, M. D. Serruya, G. M. Friehs, J. A. Mukand, M. Saleh, A. H. Caplan, A. Branner, D. Chen, R. D. Penn, and J. P. Donoghue, "Neuronal ensemble control of prosthetic devices by a human with tetraplegia," *Nature*, vol. 442, no. 7099, pp. 164–171, 2006.

[26] J. R. Wolpaw and D. J. McFarland, "Control of a two-dimensional movement signal by a noninvasive brain-computer interface in humans," *Proceedings of the National Academy of Sciences of the United States of America*, vol. 101, no. 51, pp. 17 849–17 854, 2004.

[27] J. R. Wolpaw, "Brain–computer interfaces as new brain output pathways," *The Journal of physiology*, vol. 579, no. 3, pp. 613–619, 2007.

[28] L. F. Haas, "Hans berger (1873–1941), richard caton (1842–1926), and electroencephalography," *Journal of Neurology, Neurosurgery & Psychiatry*, vol. 74, no. 1, pp. 9–9, 2003.

[29] F. Popescu, S. Fazli, Y. Badower, B. Blankertz, and K.-R. Müller, "Single trial classification of motor imagination using 6 dry eeg electrodes," *PloS one*, vol. 2, no. 7, p. e637, 2007.

[30] M. Okamoto, H. Dan, K. Sakamoto, K. Takeo, K. Shimizu, S. Kohno, I. Oda, S. Isobe, T. Suzuki, K. Kohyama *et al.*, "Three-dimensional probabilistic anatomical cranio-cerebral correlation via the international 10–20 system oriented for transcranial functional brain mapping," *Neuroimage*, vol. 21, no. 1, pp. 99–111, 2004.

[31] R. Kus, D. Valbuena, J. Zygierewicz, T. Malechka, A. Graeser, and P. Durka, "Asynchronous bci based on motor imagery with automated calibration and neurofeedback training," *IEEE Transactions on Neural Systems and Rehabilitation Engineering*, vol. 20, no. 6, pp. 823–835, 2012.

[32] G. Pfurtscheller and C. Neuper, "Motor imagery activates primary sensorimotor area in humans," *Neuroscience letters*, vol. 239, no. 2, pp. 65–68, 1997.

[33] H. Yuan, A. Doud, A. Gururajan, and B. He, "Cortical imaging of event-related (de) synchronization during online control of brain-computer interface using minimum-norm estimates in frequency domain," *IEEE Transactions on Neural Systems and Rehabilitation Engineering*, vol. 16, no. 5, pp. 425–431, 2008.

[34] G. Pfurtscheller and C. Neuper, "Motor imagery and direct brain-computer communication," *Proceedings of the IEEE*, vol. 89, no. 7, pp. 1123–1134, 2001.

[35] D. J. McFarland, L. A. Miner, T. M. Vaughan, and J. R. Wolpaw, "Mu and beta rhythm topographies during motor imagery and actual movements," *Brain topography*, vol. 12, no. 3, pp. 177–186, 2000.

[36] D. J. McFarland, W. A. Sarnacki, and J. R. Wolpaw, "Electroencephalographic (eeg) control of three-dimensional movement," *Journal of neural engineering*, vol. 7, no. 3, p. 036007, 2010.

[37] B. Blankertz, C. Sannelli, S. Halder, E. M. Hammer, A. Kübler, K.-R. Müller, G. Curio, and T. Dickhaus, "Neurophysiological predictor of smr-based bci performance," *Neuroimage*, vol. 51, no. 4, pp. 1303–1309, 2010.

[38] G. Pfurtscheller and F. L. Da Silva, "Event-related eeg/meg synchronization and desynchronization: basic principles," *Clinical neurophysiology*, vol. 110, no. 11, pp. 1842–1857, 1999.

[39] F.-B. Vialatte, M. Maurice, J. Dauwels, and A. Cichocki, "Steady-state visually evoked potentials: focus on essential paradigms and future perspectives," *Progress in neurobiology*, vol. 90, no. 4, pp. 418–438, 2010.

[40] J.-F. Cardoso, "High-order contrasts for independent component analysis," *Neural computation*, vol. 11, no. 1, pp. 157–192, 1999.

[41] T.-P. Jung, S. Makeig, C. Humphries, T.-W. Lee, M. J. Mckeown, V. Iragui, and T. J. Sejnowski, "Removing electroencephalographic artifacts by blind source separation," *Psychophysiology*, vol. 37, no. 2, pp. 163–178, 2000.

[42] R. J. Croft and R. J. Barry, "Removal of ocular artifact from the eeg: a review," *Neurophysiologie Clinique/Clinical Neurophysiology*, vol. 30, no. 1, pp. 5–19, 2000.

[43] T.-P. Jung, C. Humphries, T.-W. Lee, S. Makeig, M. J. McKeown, V. Iragui, and T. J. Sejnowski, "Removing electroencephalographic artifacts: comparison between ica and pca," in *Neural Networks for Signal Processing VIII, 1998. Proceedings of the 1998 IEEE Signal Processing Society Workshop*. IEEE, 1998, pp. 63–72.

[44] Z. J. Koles, "The quantitative extraction and topographic mapping of the abnormal components in the clinical eeg," *Electroencephalography and clinical Neurophysiology*, vol. 79, no. 6, pp. 440–447, 1991.

[45] A. Schlögl, P. Anderer, S. Roberts, M. Pregenzer, and G. Pfurtscheller, "Artefact detection in sleep eeg by the use of kalman filtering," in *Proceedings EMBEC*, vol. 99. Citeseer, 1999, pp. 1648–1649.

[46] A. Jain and D. Zongker, "Feature selection: Evaluation, application, and small sample performance," *IEEE transactions on pattern analysis and machine intelligence*, vol. 19, no. 2, pp. 153–158, 1997.

[47] D. Garrett, D. A. Peterson, C. W. Anderson, and M. H. Thaut, "Comparison of linear, nonlinear, and feature selection methods for eeg signal classification," *IEEE Transactions on neural systems and rehabilitation engineering*, vol. 11, no. 2, pp. 141–144, 2003.

[48] M. A. Hall, "Correlation-based feature selection of discrete and numeric class machine learning," 2000.

[49] P. Chum, S.-M. Park, K.-E. Ko, and K.-B. Sim, "Optimal eeg feature extraction based on r-square coefficients for motor imagery bci system," in *Control, Automation and Systems (ICCAS), 2012 12th International Conference on*. IEEE, 2012, pp. 754–758.

[50] G. Pfurtscheller, C. Neuper, D. Flotzinger, and M. Pregenzer, "Eeg-based discrimination between imagination of right and left hand movement," *Electroencephalography and clinical Neurophysiology*, vol. 103, no. 6, pp. 642–651, 1997.

[51] M. Pregenzer and G. Pfurtscheller, "Frequency component selection for an eeg-based brain to computer interface," *IEEE Transactions on Rehabilitation Engineering*, vol. 7, no. 4, pp. 413–419, 1999.

[52] C. Neuper, R. Scherer, M. Reiner, and G. Pfurtscheller, "Imagery of motor actions: Differential effects of kinesthetic and visual–motor mode of imagery in single-trial eeg," *Cognitive brain research*, vol. 25, no. 3, pp. 668–677, 2005.

[53] A. R. Satti, D. Coyle, and G. Prasad, "Spatio-spectral & temporal parameter searching using class correlation analysis and particle swarm optimization for a brain computer interface," in *Systems, Man and Cybernetics, 2009. SMC 2009. IEEE International Conference on*. IEEE, 2009, pp. 1731–1735.

[54] B. Dal Seno, M. Matteucci, and L. Mainardi, "A genetic algorithm for automatic feature extraction in p300 detection," in *Neural Networks, 2008. IJCNN 2008.(IEEE World Congress on Computational Intelligence). IEEE International Joint Conference on*. IEEE, 2008, pp. 3145–3152.

[55] R. Sharma and R. B. Pachori, "Classification of epileptic seizures in eeg signals based on phase space representation of intrinsic mode functions," *Expert Systems with Applications*, vol. 42, no. 3, pp. 1106–1117, 2015.

[56] R. J. Martis, U. R. Acharya, J. H. Tan, A. Petznick, R. Yanti, C. K. Chua, E. K. Ng, and L. Tong, "Application of empirical mode decomposition (emd) for automated detection of epilepsy using eeg signals," *International journal of neural systems*, vol. 22, no. 06, p. 1250027, 2012.

[57] Z. Ni, L. Wang, J. Meng, F. Qiu, and J. Huang, "Eeg signal processing in anesthesia feature extraction of time and frequency parameters," *Procedia Environmental Sciences*, vol. 8, pp. 215–220, 2011.

[58] J. I. Salisbury and Y. Sun, "Assessment of chaotic parameters in nonstationary electrocardiograms by use of empirical mode decomposition," *Annals of biomedical engineering*, vol. 32, no. 10, pp. 1348–1354, 2004.

[59] B. Samanta, "Morphological processing of physiological signals for feature extraction," in *Engineering in Medicine and Biology Society, 2009. EMBC 2009. Annual International Conference of the IEEE*. IEEE, 2009, pp. 324–327.

[60] M. Agarwal and R. Jain, "Ensemble empirical mode decomposition: An adaptive method for noise reduction," *IOSR J. Electron. Commun. Eng*, vol. 5, pp. 60–65, 2013.

[61] T. Juric, M. Bonkovic, and M. Rogic, "Application of eemd-ica algorithm to emg signals measured in laryngeal muscles," in *Software, Telecommunications and Computer Networks (SoftCOM), 2013 21st International Conference on*. IEEE, 2013, pp. 1–4.

[62] F. Riaz, A. Hassan, S. Rehman, I. K. Niazi, and K. Dremstrup, "Emd-based temporal and spectral features for the classification of eeg signals using supervised learning," *IEEE Transactions on Neural Systems and Rehabilitation Engineering*, vol. 24, no. 1, pp. 28–35, 2016.

[63] B. Boashash, "Estimating and interpreting the instantaneous frequency of a signal. i. fundamentals," *Proceedings of the IEEE*, vol. 80, no. 4, pp. 520–538, 1992.

[64] A. Schlögl, F. Lee, H. Bischof, and G. Pfurtscheller, "Characterization of four-class motor imagery eeg data for the bci-competition 2005," *Journal of neural engineering*, vol. 2, no. 4, p. L14, 2005.

[65] M. Kaper, P. Meinicke, U. Grossekathoefer, T. Lingner, and H. Ritter, "Bci competition 2003-data set iib: support vector machines for the p300 speller paradigm," *IEEE Transactions on Biomedical Engineering*, vol. 51, no. 6, pp. 1073–1076, 2004.

[66] K.-R. Müller, M. Krauledat, G. Dornhege, G. Curio, and B. Blankertz, "Machine learning techniques for brain-computer interfaces," *Biomed. Tech*, vol. 49, no. 1, pp. 11–22, 2004.

[67] S. G. Mason and G. E. Birch, "A general framework for brain-computer interface design," *IEEE transactions on neural systems and rehabilitation engineering*, vol. 11, no. 1, pp. 70–85, 2003.

[68] B. Kemp, A. Värri, A. C. Rosa, K. D. Nielsen, and J. Gade, "A simple format for exchange of digitized polygraphic recordings," *Electroencephalography and clinical neurophysiology*, vol. 82, no. 5, pp. 391–393, 1992.

[69] A. Schlögl, "Gdf-a general dataformat for biosignals," *arXiv preprint cs/0608052*, 2006.

[70] K. I. Diamantaras and S. Y. Kung, *Principal component neural networks: theory and applications*. John Wiley & Sons, Inc., 1996.

[71] D.-x. Zhang, X.-p. Wu, and X.-j. Guo, "The eeg signal preprocessing based on empirical mode decomposition," in *Bioinformatics and Biomedical Engineering, 2008. ICBBE 2008. The 2nd International Conference on*. IEEE, 2008, pp. 2131–2134.

[72] Y. Song, P. Liò *et al.*, "A new approach for epileptic seizure detection: sample entropy based feature extraction and extreme learning machine," *Journal of Biomedical Science and Engineering*, vol. 3, no. 06, p. 556, 2010.

[73] P. Bhuvaneswari and J. S. Kumar, "Support vector machine technique for eeg signals," *International Journal of Computer Applications*, vol. 63, no. 13, 2013.